ANL-5850
Reactors - Power
AEC Research and
Development Report

ARGONNE NATIONAL LABORATORY
P. O. Box 299
Lemont, Illinois

ANALYSES OF EXPERIMENTAL POWER-REACTIVITY FEEDBACK TRANSFER FUNCTIONS FOR A NATURAL CIRCULATION BOILING WATER REACTOR

by

J. A. DeShong, Jr., and W. C. Lipinski

Reactor Engineering Division

July, 1958

Operated by The University of Chicago
under
Contract W-31-109-eng-38

DISCLAIMER

TABLE OF CONTENTS

LIST OF TABLES

LIST OF FIGURES

NOMENCLATURE

b	Boundary coefficient, ft^3 sec/psi (See Appendix D)
d	Flashing coefficient, ft^3 sec/psi (See Appendix D)
$H(S)$	Heat transfer function
h_{FW}	Specific feedwater enthalpy, BTU/lb
h_s	Specific steam enthalpy, BTU/lb
h_w	Specific water enthalpy, BTU/lb
K_{BP}	Bypass valve coefficient, lb/(sec)(psi)
m_1	Steam mass in vessel, lb
$\dot{m}_2$	Steam load, lb/sec
M	Mass of water in vessel, lb
M_c	Mass of water in core, lb
M_B	Mass of water in boiling portion of core, lb
M_{NB}	Mass of water in non-boiling portion of core, lb
$\dot{M}_{FW}$	Feedwater flow, lb/sec
$\dot{M}_R$	Recirculation flow, lb/sec
MW	Thermal power, megawatts
$\dot{N}$	Normalized reactor power ($\dot{N}_0 = 1$)
p	Pressure, psi
r_r	Recirculating-water to feed-water flow ratio
S	Laplace operator Complex frequency variable ($j\omega$) for frequency domain
T_h	Heat transfer time constant, sec

T_{pv} Heat transfer time constant, sec

T_r Recirculation time constant, sec

V Power void coefficient $(ft^3/MW)MW$

V_0 Total steam voids, ft^3

Greek Symbols:

β_T Total delayed neutron fraction

δK Net reactivity, dollars

δK_v Reactivity in voids, dollars

$K_{\delta K}$ Void reactivity coefficient, dollars/ft^3

γ Steam constant, lb/psi (See Appendix C)

η Steam constant, lb/psi (See Appendix C)

ω Frequency, rad/sec

σ Steaming rate, lb/sec

ρ_s Specific steam density, lb/ft^3

τ Steam transit time constant, sec

θ Temperature, °F

Note: Time derivatives are indicated by a dot above the symbol.

ANALYSES OF EXPERIMENTAL POWER-REACTIVITY FEEDBACK TRANSFER FUNCTIONS FOR A NATURAL CIRCULATION BOILING WATER REACTOR

J. A. DeShong, Jr., and W. C. Lipinski

ABSTRACT

Experimental power-reactivity feedback transfer functions were calculated from the EBWR power transfer function measurements. A simplified model of the EBWR kinetics was developed, using an analog computer, and an analytic expression was obtained for the feedback function. The analytic solution was fitted to the experimental functions to obtain power coefficients and time constants for various modes of operation.

These data were extrapolated, and a power transfer function was predicted for 40 MW. The reactor function was measured and compared with the prediction. A stability study was carried out, using open loop transfer functions containing the experimental feedback functions. Extrapolation of the gain and phase margins indicated stability to at least 66 MW. The reactor was successfully operated at 61.7 MW following this, with power limited by the capacity of the feedwater pumps.

The use of the simplified model for parameter studies is demonstrated by a series of calculations to evaluate the effect of heat transfer time constant on stability.

I. INTRODUCTION

One of the first major efforts of the EBWR experimental program was a stability investigation whose objective was to evaluate maximum stable power output capabilities of the reactor by the use of small-signal linear feedback control theory.[1] The first phase of the program was devoted to determination of the performance of the reactor by measuring its power transfer functions for many different values of power parameters, all within the limits prescribed by the safeguard report.[2] The

---

[1] H. Chestnut and R. W. Mayer, "Servomechanisms and Regulating System Design" (New York: J. Wiley and Sons, Inc., 1951).

[2] J. M. West, J. R. Dietrich, A. S. Jameson, G. A. Anderson, J. M. Harrer and H. F. Brush, "Hazard Summary Report on the Experimental Boiling Water Reactor (EBWR)." ANL-5781.

equipment and methods used to make these measurements are covered in detail in a preceding ANL report which also contains the resulting power transfer functions.[3] Table I is a summary of this data. Such functions are a convenient way of expressing reactor kinetics.[4] As used here they may be defined as the amplitude and phase relation of the sinusoidal variation in flux or power output with respect to the sinusoidal reactivity input driving function.

The reactor power transfer function, P_1, is defined as the zero-power function modified by power-to-reactivity feedback.[3]

Then:

$$P_1 = \frac{G}{1 + GH_1} = \frac{\text{Flux Output}}{\text{Reactivity Input}} \quad , \qquad (1)$$

where G is the zero-power function (normalized with respect to β and flux), and H_1 is the power-to-reactivity feedback function for the specified reactor power parameters. Figure 1 illustrates this schematically. Figure 2 shows the G function amplitude and phase, respectively.[3]

Many techniques may be used to determine quantitative stability from P_1.[1,4,5,6] The log polar plane or "Nichols" chart was used for plotting frequency loci in the EBWR investigations.[1] This makes use of the open loop function which is the zero-power function, G, multiplied by the feedback function, H_1.

Direct measurement of the GH_1 function was not feasible, and calculation of H_1 from thermodynamic data was difficult because of its complex nature.[7] In fact, one purpose of the program was to provide data to orient such calculations made on a simplified theoretical model which is described in a later section. For the above reasons the experimental GH_1 was calculated, using P_1 and G. The experimental H_1 was then obtained from GH_1 to permit its correlation with the analytic H_1 of the model and to provide a means for extrapolation to higher power levels.

---

[3] J. A. DeShong, Jr., "Power Transfer Functions of the EBWR Obtained Using a Sinusoidal Reactivity Driving Function," ANL-5798.

[4] J. M. Harrer and J. A. DeShong, Jr., "Discontinuous Servo for Power Reactor Control," Nucleonics 12 (1), 44 (1954).

[5] H. W. Bode, "Network Analysis and Feedback Amplifier Design." (New York: D. Van Nostrand Co., Inc., 1945).

[6] M. A. Schultz, "Control of Nuclear Reactors and Power Plants." (New York: McGraw-Hill Book Co., Inc., 1955).

[7] E. S. Beckjord, "Dynamic Analysis of Natural Circulation Boiling Water Power Reactors." ANL-5799 (March 1958).

TABLE I

POWER FUNCTION MEASUREMENTS

TEST PARAMETERS (EQUILIBRIUM XENON EXCEPT TEST NO. 15)	TEST NUMBER													
	1	2	3	4	5	6	7	8	9	10	11	13	14	15
POWER, mw	ZERO (6 kw)	5.4	9.7	20	20	5.7	5.2	5.2	5.1	20	20	20	33	50
PRESSURE, psig	150	550	550	550	550	550	310	300	130	300	550	310	550	600
BORON	NO	NO	NO	NO	YES	YES	YES	NO	NO	NO	NO	NO	NO	NO
CENTER ROD, in.	13.6	13.6	13.8	23.7	23.7	23.7	23.9	13.8	13.8	23.9	24.0	23.9	41.0	41.0
8-ROD BANK, in.	14.5	24.1	29.0	33.0	41.3	41.3	41.2	22.9	22.3	34.7	33.1	35.1	47.0	47.0
STEAM BYPASS	MANUAL	MANUAL	MANUAL	MANUAL	MANUAL	MANUAL	MANUAL	MANUAL	MANUAL	MANUAL	AUTOMATIC	AUTOMATIC	MANUAL	AUTOMATIC
PEAK REACTIVITY (%) FOR 1-inch PEAK STROKE	0.087	0.071	0.10	0.043	0.048	0.048	0.043	0.067	0.065	0.046	0.043	0.040	———	———

RATIO OF FLUX TO REACTIVITY AMPLITUDES AND RELATIVE PHASE OF FLUX TO REACTIVITY

Ratio is Given in Decibels (Zero Db. = 132) and Phase in Degrees

FREQUENCY, radians/sec	CALC.		EXPTL.		Db	Phase	Db	Phase	Db	Phase	Db	Phase	Db	Phase	Db	Phase	Db	Phase	Db	Phase	Db	Phase	Db	Phase	Db	Phase	Db	Phase	Db	Phase
	Db	Phase	Db	Phase																								
0.016	+15.8	-65	—	—	—	—	—	—	-3.6	0	-1.0	+2	+6.3	0	+6.2	-10	+2.3	-4	+0.2	0	-1.5	-5	-7.5	+9	-6.5	+17	-0.4	+10	—	—
0.032	+11.9	-53	—	—	—	—	—	—	-3.6	-10	-1.8	-12	+4.8	-15	+4.6	-16	+1.4	-12	-0.3	-8	-2.2	-12	-7.5	+11	-5.3	+16	-0.9	-6	—	—
0.063	+9.1	-44	—	—	—	—	—	—	-4.2	-17	-2.7	-13	+3.0	-20	+3.8	-20	+0.2	-15	0	-13	-3.5	-20	-5.0	—	-3.6	+10	-2.0	-18	—	—
0.126	+6.5	-37	+6.9	-41	-0.9	-19	-2.3	-17	-4.2	-14	-3.6	-15	+1.0	-23	+1.1	-22	-1.4	-18	-2.7	-18	-5.2	-22	-4.5	+5	-3.6	-5	-4.7	-20	—	—
0.252	+4.2	-30	—	—	—	—	—	—	—	—	—	—	—	—	—	—	—	—	—	—	—	—	-4.5	-10	-6.1	-16	—	—	—	—
0.314	+3.6	-28	+3.7	-28	-2.6	-15	-5.4	-13	-5.6	-12	-5.9	-12	-1.3	-17	-0.8	-16	-3.9	-13	-5.2	-14	-8.1	-14	-5.5	-6	-6.5	-16	-6.3	-20	—	—
0.63	+2.0	-20	+2.0	-19	-4.2	-4	-6.3	-7	-7.7	-6	-7.8	-5	-2.3	-3	-2.0	-1	-5.1	-1	-6.6	+2	-9.4	-2	-7.6	0	-7.5	-5	-10.7	-15	—	—
1.26	+1.0	-14	+1.1	-15	-4.0	+15	-5.9	+16	-7.4	+10	-7.4	+13	-2.3	+9	-1.3	+10	-4.8	+14	-5.4	+18	-9.4	+12	-8.1	+12	-9.2	+18	-10.7	-10	—	—
1.89	+0.7	-11	+0.5	-9	-2.9	+27	-4.8	+31	—	+24	-7.4	+28	-1.3	+20	-0.6	+16	-4.2	+27	-5.3	+28	-9.3	+23	-8.7	+20	-8.3	+25	—	—	—	—
2.52	+0.5	-9	—	—	—	—	—	—	—	—	—	—	—	—	—	—	—	—	—	—	—	—	—	—	—	—	-9.4	+35	—	—
3.14	+0.4	-8	+0.4	-8	+0.8	+30	-1.4	+43	-5.2	+46	-4.7	+50	+1.7	+16	+2.1	+16	-0.4	+36	-3.1	+46	-8.2	+45	-5.8	+51	-7.0	+47	—	—	—	—
4.4	+0.3	-8	+0.2	-6	+2.5	+16	+1.4	+33	-1.6	+58	-0.1	+57	+2.2	+5	+2.6	+6	-6.1	+29	+0.7	+43	-5.8	+65	-1.8	+55	-3.9	+64	—	—	—	—
5.0	+0.2	-7	—	—	—	—	—	—	—	—	—	—	—	—	—	—	—	—	—	—	—	—	—	—	—	—	-4.7	+75	—	—
6.28	+0.2	-7	0	-6	+2.5	+1	+3.2	+10	+3.7	+48	+3.4	+34	+1.6	-3	+1.9	-4	+2.6	+10	+3.4	+23	+1.0	+73	+2.8	+41	+2.4	+71	+2.1	+75	—	—
7.5	+0.1	-7	—	—	—	—	—	—	—	—	—	—	—	—	—	—	—	—	—	—	—	—	—	—	—	—	+6.4	+65	—	—
8.8	+0.1	-7	—	—	—	—	—	—	—	—	—	—	—	—	—	—	—	—	—	—	—	—	—	—	—	—	+8.1	+15	+6.6	+80
9.4	+0.1	-8	—	—	—	—	—	—	—	—	+3.6	+1	—	—	+0.7	-6	+1.3	-5	+1.4	-4	+6.7	+25	+4.3	+2	+6.6	—	+6.3	+3	+8.2	+90
10.7	+0.1	-8	—	—	—	—	—	—	—	—	—	—	—	—	—	—	—	—	—	—	—	—	—	—	—	—	—	—	+13.0	+10
11.0	+0.1	-8	—	—	—	—	—	—	—	—	—	—	—	—	—	—	—	—	—	—	—	—	—	—	—	—	+5.0	-7	—	—
11.6	0	-8	—	—	—	—	—	—	—	—	—	—	—	—	—	—	—	—	—	—	—	—	—	—	—	—	—	—	+12.3	0
12.5	0	-8	-0.5	-8	+0.5	-10	+0.1	-10	+1.3	-11	+2.0	-5	+0.2	-6	+0.1	-6	-0.8	-7	-0.4	-9	+4.0	-6	+2.0	-12	+3.9	-10	+2.1	-6	+4.8	-10
15.7	0	-10	—	—	—	—	—	—	—	—	—	—	—	—	—	—	—	—	—	—	+2.1	-9	+0.7	-15	—	—	—	—	—	—
18.8	-0.1	-11	—	—	—	—	—	—	—	—	—	—	—	—	—	—	—	—	—	—	+1.2	-9	+0.3	-17	—	—	+1.5	-9	+4.0	-20
25.1	-0.2	-13	-0.5	-13	-0.6	-16	-1.5	-17	-0.2	-19	-0.3	-11	-0.4	-14	-0.5	-14	-2.4	-16	-1.6	-15	+0.3	-12	—	—	—	—	+1.8	-10	-0.3	-15

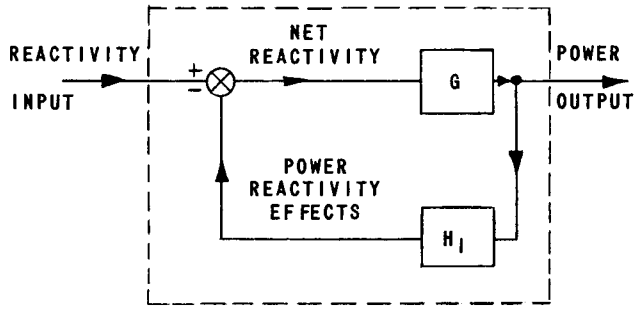

FIG. 1
POWER-TO-REACTIVITY FEEDBACK SCHEMATIC

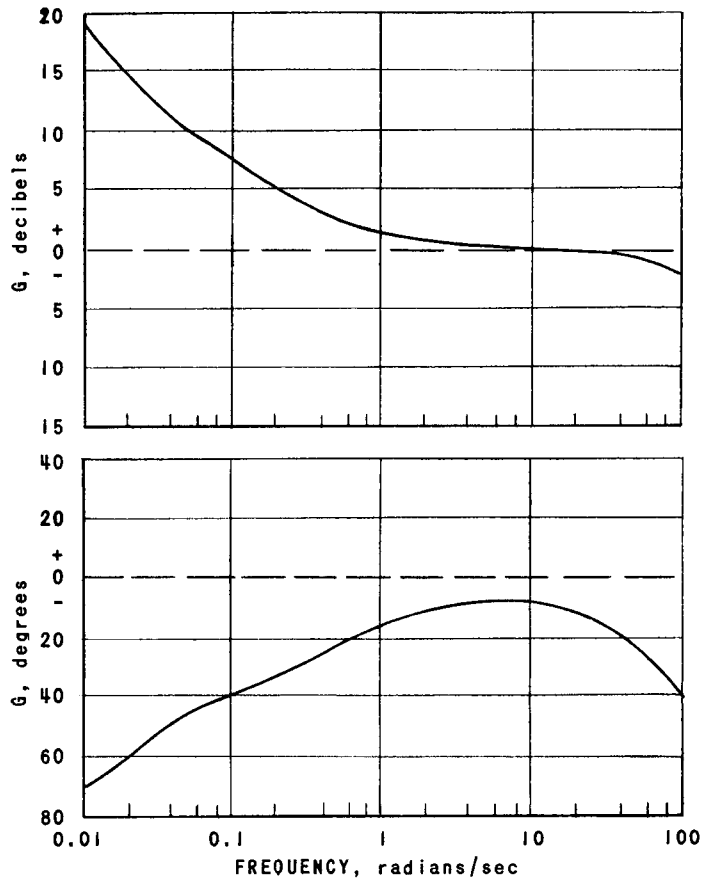

$$G(s) = \frac{\dot{N}(s)-\dot{N}_o}{\delta K(s)/\beta_T} = \frac{\dot{N}_o}{S\left[\frac{\ell^*}{\beta_T} + \Sigma \frac{\beta_i/\beta_T\lambda_i}{1 + s/\lambda_i}\right]}$$

FIG. 2
ZERO POWER FREQUENCY RESPONSE

II. EXPERIMENTAL TRANSFER FUNCTIONS

A very high degree of accuracy is required for measurements which are to be used for calculations of H from the G and P functions, particularly at the higher frequencies where P is nearly equal to the G function. Physically, P must equal G at very high frequencies, since the power feedback and GH become small with respect to one. Rewriting (1) gives:

$$H_1 = P_1^{-1} - G^{-1} \quad . \tag{2}$$

For $GH_1 << 1$

$$P_1 = \frac{G}{1 + GH_1} \cong G \quad . \tag{3}$$

It may be seen from equation (2) that phase errors of a few degrees and amplitude errors of several per cent in P_1 can change the calculated value of H_1 by large amounts, since H_1 is the difference between two nearly equal quantities, both much larger than H_1.

The experimental P functions used in this work were determined with an accuracy of about ±5 per cent in amplitude and ±2 degrees in phase. Even this accuracy was insufficient, so it was necessary to develop a means for smoothing the data. Also, the uncertainties in the data included a normalizing factor which sets the reference amplitude of the P function with respect to the G function. The factor is determined by the reactivity input magnitude which could not be measured with very good accuracy because the rod reactivity calibrations are a function of the moderator density, which, in turn, varies with the void content of the core.[8]

A method which resolves both the above difficulties utilizes an inversion of the log polar plane or "Nichols Chart." Figure 3 shows the result obtained by calculating (1 + GH) from the data for test No. 10 in Table I and plotting it on the inverted log polar plane. On such a plot it is possible to draw a smooth curve through the experimental points to provide data smoothing. Variation in the normalizing factor is accomplished simply by sliding the entire curve up or down along the (1 + GH) axis. When this is done, the shape of the GH amplitude curve is altered, while the GH phase curve is comparatively unchanged. Then, by application of the minimum phase shift theorem which relates amplitude and phase, it is possible to select the value of normalizing factor which provides the best agreement between the amplitude and phase curves.[9] G is then subtracted from the resulting GH function to obtain the experimental reactivity feedback function, H. Table II and Figs. 4 and 5 show the experimental H functions for EBWR in the form of Bode phase and amplitude curves obtained using the data from Table I and processing as indicated above.[5]

---

[8] J. A. Thie, "EBWR Physics Experiments," ANL-5711

[9] H. W. Bode, "Relations Between Attenuation and Phase in Feedback Amplifier Design," Bell System Technical Journal, 19, 421 (July 1940).

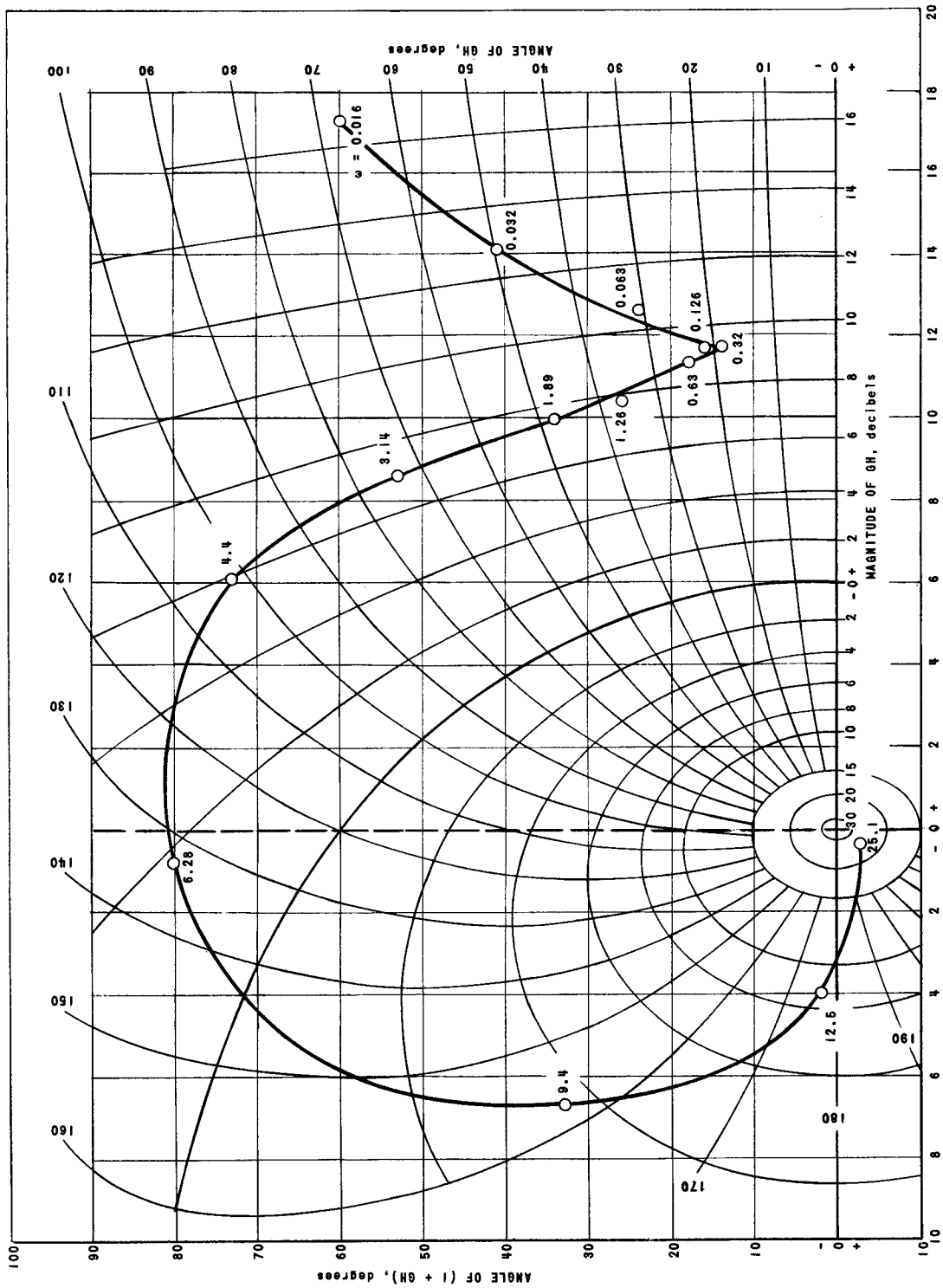

FIG. 3
DETERMINATION OF EXPERIMENTAL GH

TABLE II

EXPERIMENTAL FEED-BACK FUNCTION DATA

TEST PARAMETERS (EQUILIBRIUM XENON EXCEPT TEST NO. 15)	TEST NUMBER										
	2	3	4	5	6	7	8	9	10	14	15
POWER, mw	5.4	9.7	20	20	5.7	5.2	5.2	5.1	20	33	50
PRESSURE, psig	550	550	550	550	550	310	300	130	300	550	600
BORON	NO	NO	NO	YES	YES	YES	NO	NO	NO	NO	NO

RATIO OF REACTIVITY TO FLUX AMPLITUDES AND RELATIVE PHASE OF REACTIVITY TO FLUX

Ratio is Given in Decibels (Zero Db. = 0.00755) And Phase in Degrees

FREQUENCY, radians/sec.	Db	Phase	Db	Phase	Db	Phase	Db	Phase	Db	Phase	Db	Phase	Db	Phase	Db	Phase	Db	Phase	Db	Phase	Db	Phase
0.016	—	—	—	—	+2.4	-6	+0.5	-10	-7.6	-21	-7.6	-8	-3.4	-7	-0.8	-9	+1.0	-2	+0.1	-19	—	—
0.032	—	—	—	—	+2.0	+3	+0.4	+3	-7.8	-8	-7.5	-5	-3.3	-2	-1.1	-4	+1.0	+4	-0.4	-5	—	—
0.063	—	—	—	—	+1.9	+7	+0.7	+3	-7.6	0	-9.3	0	-3.2	+1	-0.8	-1	+1.6	+9	-0.4	+8.6	—	—
0.126	-3.4	+6	-1.1	+6	+2.7	+4	+0.9	+5	-7.0	+7	-7.0	+5	-2.5	+5	-0.6	+8	+3.7	+16	+0.7	+14	—	—
0.314	-2.8	+3	+1.9	+5	+3.1	+4	+2.6	+4	-5.5	+3	-6.6	-1	-0.5	+3	+1.6	+6	+6.5	+8	+4.4	+17	—	—
0.63	-1.0	-11	+2.3	-1	+4.6	0	+4.6	-2	-4.5	-21	-5.5	-17	+0.7	-13	+3.2	-15	+7.6	-1	+7.9	+15	—	—
1.26	-1.4	-42	+2.2	-36	+4.8	-23	+4.1	-28	-4.4	-44	-5.9	-55	+0.4	-38	+1.6	-41	+7.5	-21	+8.1	+0.4	—	—
1.89	-1.2	-67	+1.7	-61	+4.6	-42	+4.8	-48	-4.4	-72	-6.2	-75	+0.5	-60	+2.0	-55	+7.6	-36	+7.5	-23	—	—
3.14	-4.0	-105	-0.5	-94	+4.2	-75	+3.4	-84	-7.7	-114	-7.8	-116	-2.4	-99	+1.3	-87	+7.2	-65	+7.2	-67	—	—
4.4	-7.5	-126	-3.8	-113			+0.9	-114	-11.0	-134	-10.2	-138	-4.8	-116	-1.8	-110	+6.2	-94	+6.3	-97	—	—
6.28	-11.3	-151	-8.6	-139	-1.4	-130	-3.7	-129	-15.4	-153	-14.6	-160	-9.1	-135	-5.9	-131	+2.1	-127	+3.0	-136	—	—
8.8	—	—	—	—	—	—	—	—	—	—	—	—	—	—	—	—	—	—	—	—	-0.3	-147
9.4	—	—	—	—	-7.7	-160	-9.0	-155	—	—	—	—	-16.9	-160	-16.9	-149	-4.1	-158	-5.7	-160	0	-155
10.7	—	—	—	—	—	—	—	—	—	—	—	—	—	—	—	—	—	—	—	—	-2.2	-167
11.6	—	—	—	—	—	—	—	—	—	—	—	—	—	—	—	—	—	—	—	—	-2.4	-170
12.5	-23.4	-185	—	—	-16.3	-183	-12.9	-156	—	—	—	—	—	—	—	—	-8.1	-169	-9.5	-165	-7.4	-175
15.7	—	—	—	—	—	—	—	—	—	—	—	—	—	—	—	—	-12.2	-177	—	—	—	—
18.8	—	—	—	—	—	—	—	—	—	—	—	—	—	—	—	—	-16.2	-185	—	—	-7.9	-185
25.1	—	—	—	—	-25.1	-224	—	—	-31.8	-205	—	—	—	—	—	—	-23.1	-203	—	—	-25.3	-267

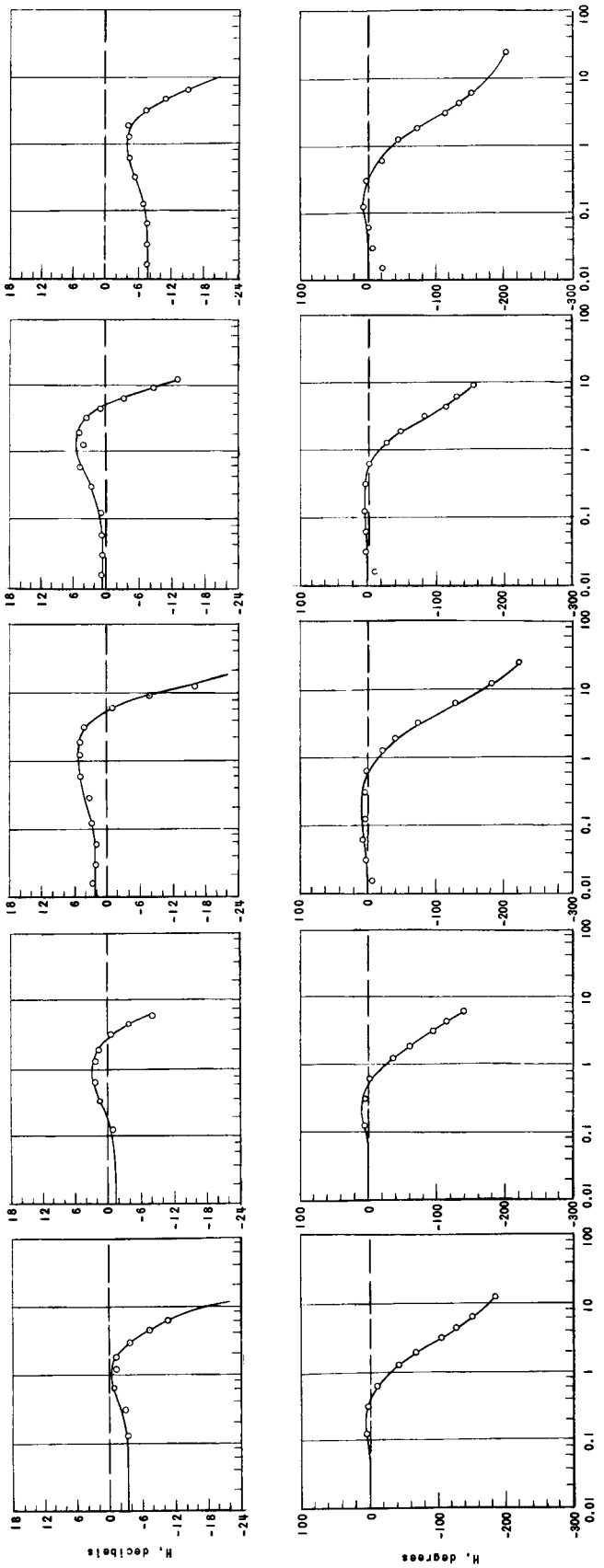

FIG. 4
POWER EFFECTS ON FEEDBACK FUNCTION AT 550 psi

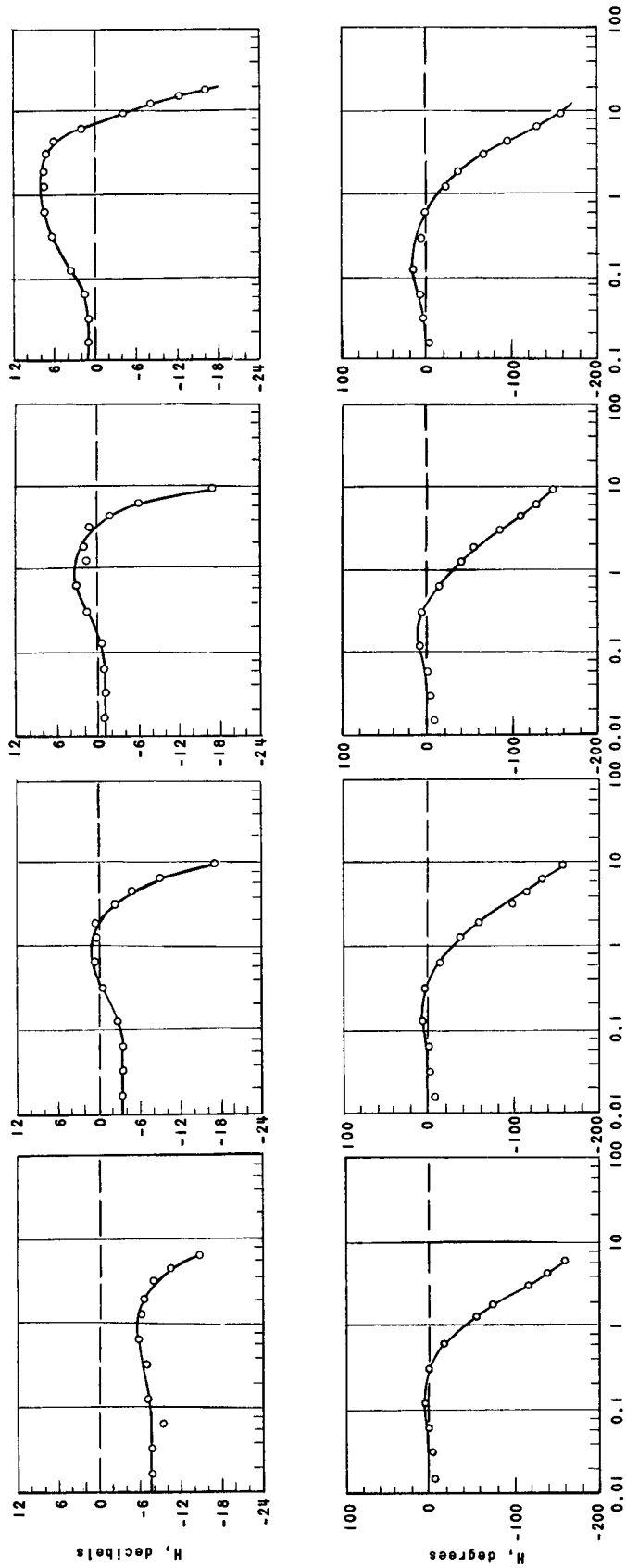

FIG. 5
PRESSURE EFFECTS ON FEEDBACK FUNCTION

III. THE BOILING REACTOR MODEL WITH SOME ANALYTIC SOLUTIONS

Figure 6 shows a preliminary model of a natural circulation boiling water reactor plant in block diagram form.[7] The transfer function measurements made on EBWR were performed with feedwater flow held constant, manual pressure control, and with the turbine off; therefore, that portion of the figure outside of the dashed section of Fig. 6 can be neglected in determining an analytical expression for the feedback transfer function from reactor power output to reactivity input. The resulting reactor model is shown in Fig. 7.

The preliminary heat transfer model, calculated using the method of ANL-5799, is given by:

$$H(S)_{(\text{heat transfer})} = \frac{(1 + \frac{S}{16})}{(1 + \frac{S}{1.7})(1 + \frac{S}{18})} \quad . \tag{4}$$

The combined effect of the above heat transfer function and the power void transfer function is to produce a 12-db-per-octave falloff in the frequency region just above 8 rad/sec. The feedback transfer functions derived earlier in Part II require an 18-db-per-octave falloff for this frequency region. The difference of 6 db per octave represents a third time constant which does not appear in the preliminary model. There is evidence that the additional time constant is associated with effects related to power transfer in the non-boiling portion of the core (see Section IV.) An investigation of the above effects is under way. The third time constant was included by removing the lead time constant of equation (4) as shown by the heat transfer box in Fig. 7.

The model of Fig. 7 was analyzed by means of a large, precision analog computer over the frequency range of 0.01 rad/sec to 100 rad/sec. It was established that the temperature coefficient had negligible effect above 0.01 rad/sec. Therefore, the effect of temperature coefficient was neglected in the derivations that follow. Figure 7 can be further simplified by reducing the minor loop which relates steam generation to pressure rate as shown in Fig. 8. The derivation for the forward portion of this loop is given in Appendix A.

$$\frac{\dot{p}}{\dot{m}_1 + \dot{m}_2}(S) = \frac{S(1 + S T_r)}{K_{BP}\left[S^2 \frac{\gamma T_r}{K_{BP}} + S\left(\frac{\eta}{K_{BP}} + T_r\right) + 1\right]} \tag{5}$$

$$\frac{\dot{p}}{\dot{m}_1 + \dot{m}_2}(S) = \frac{S(1 + ST_r)}{K_{BP}(1 + ST_1)(1 + ST_2)} \tag{6}$$

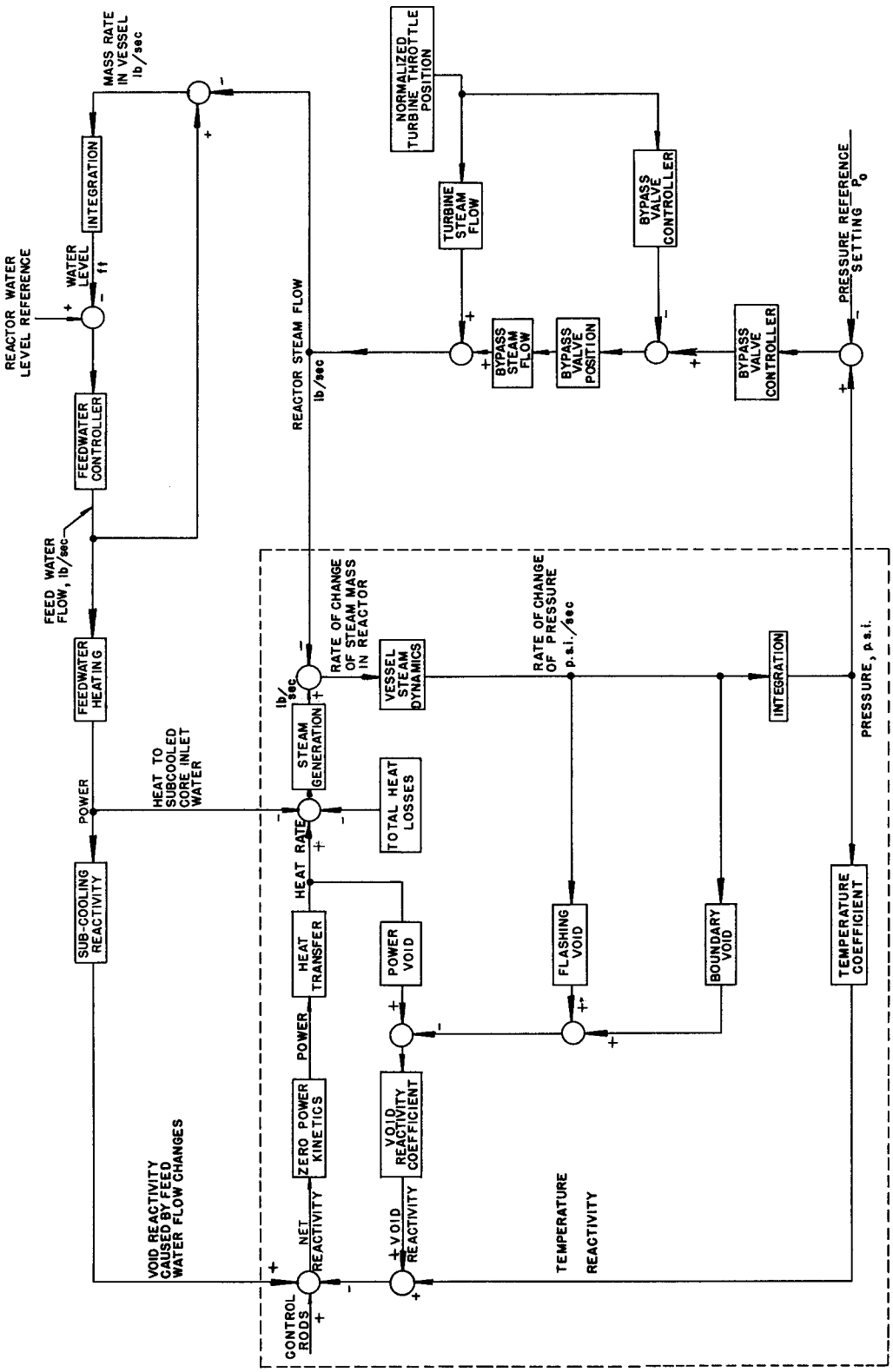

FIG. 6

PLANT BLOCK DIAGRAM OF E B W R

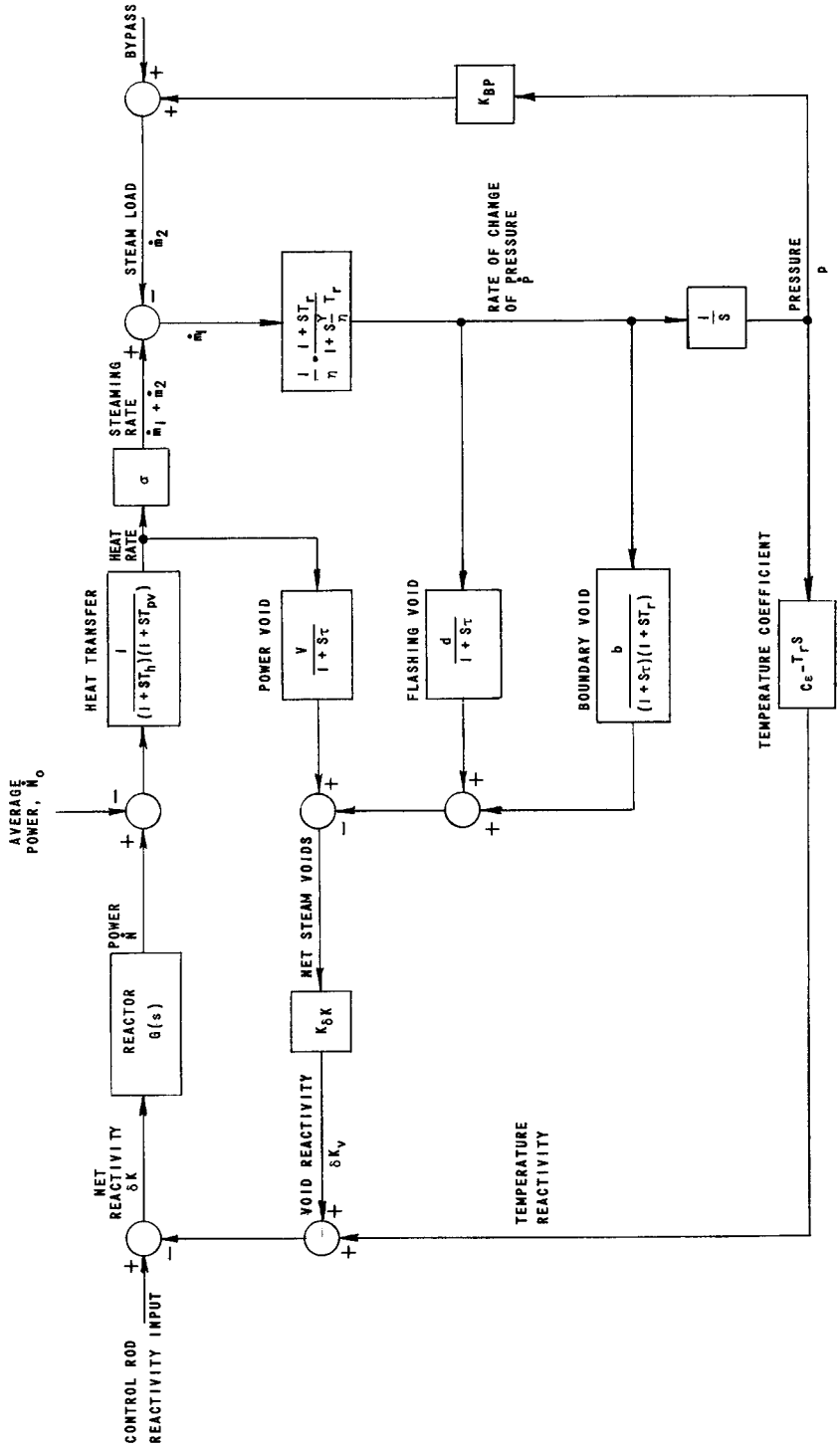

FIG. 7
LINEARIZED INCREMENTAL - SIGNAL REACTOR MODEL

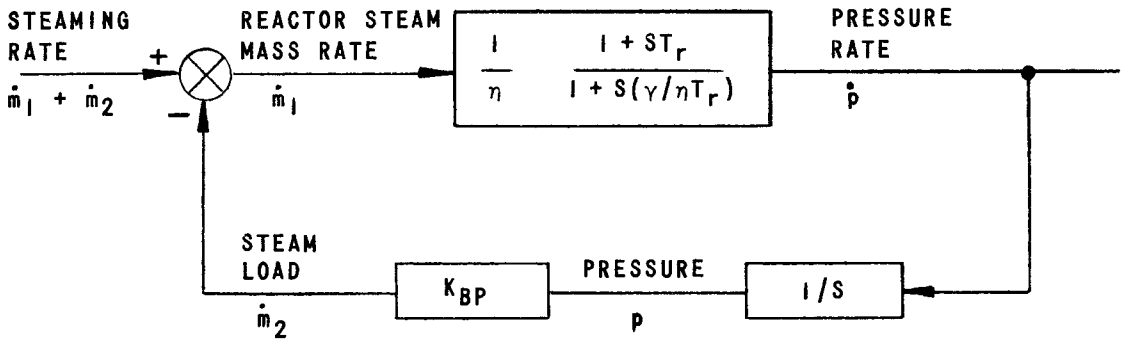

$$\frac{\dot{p}}{\dot{m}_1 + \dot{m}_2}(S) = \frac{S(1 + ST_r)}{K_{BP}\left[1 + S(\eta/K_{BP})\right]\left[1 + S(\gamma T_r/\eta)\right]}$$

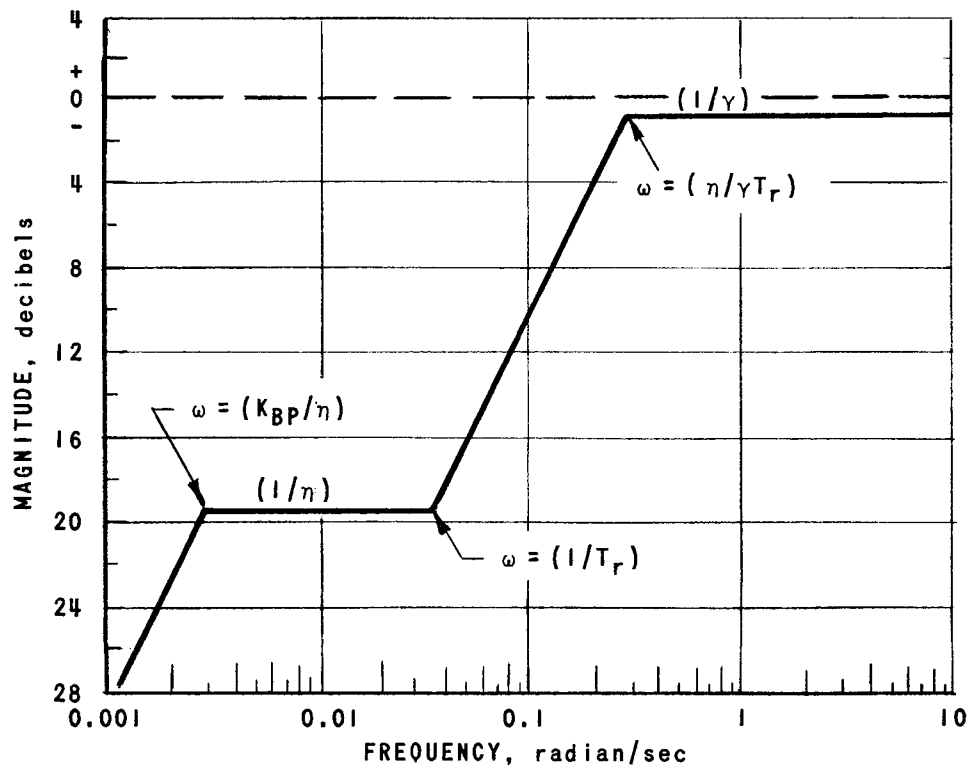

FIG. 8
PRESSURE RATE ANALYSIS

where

$$T_1 = \frac{1}{2}\left[\frac{\eta}{K_{BP}} + T_r - \sqrt{\left(\frac{\eta}{K_{BP}} + T_r\right)^2 - 4\frac{\gamma T_r}{K_{BP}}}\right] \tag{7}$$

$$T_2 = \frac{1}{2}\left[\frac{\eta}{K_{BP}} + T_r + \sqrt{\left(\frac{\eta}{K_{BP}} + T_r\right)^2 - 4\frac{\gamma T_r}{K_{BP}}}\right] . \tag{8}$$

Equation (5) can be approximated as shown by equation (9).

$$\frac{p}{\dot{m}_1 + \dot{m}_2}(S) \approx \frac{S\,(1 + ST_r)}{K_{BP}\left(1 + S\frac{\eta}{K_{BP}}\right)\left(1 + S\frac{\gamma T_r}{\eta}\right)} . \tag{9}$$

The Bode diagram for equation (9) is shown in Fig. 8.[5]

Equation (9) for the transfer function of Fig. 8, allows Fig. 7 to be reduced as shown in Fig. 9. The overall feedback transfer function from reactor power, $\dot{N}$, to void reactivity, δK_v, is defined as H(S). It is derived in Appendix B and is given by equations (10) and(10a):

$$H(S) = \frac{\delta K_v(S)}{\dot{N}(S)} \tag{10}$$

$$H(S) = \frac{K_{\delta K V}\left[\frac{T_r}{K_{BP}}\left(\gamma - \frac{\sigma d}{V}\right)S^2 + \left(\frac{\eta}{K_{BP}} + \frac{\gamma}{\eta}T_r + \frac{\sigma(b+d)}{V\,K_{BP}}\right)S + 1\right]}{(1 + ST_h)\,(1 + ST_{pv})\,(1 + S\tau)\left(1 + S\frac{\eta}{K_{BP}}\right)\left(1 + S\frac{\gamma}{\eta}T_r\right)} . \tag{10a}$$

Equation (10a) can be further simplified by noting that the frequency corresponding to the $\frac{K_{BP}}{\eta}$ break point is approximately one-half decade below 0.01 rad/sec, the lowest frequency measured experimentally. For frequencies greater than $\frac{K_{BP}}{\eta}$ equation (9) reduces to equation (11):

$$\frac{\dot{p}}{\dot{m}_1 + \dot{m}_2}(S) = \frac{(1 + ST_r)}{\eta\left(1 + S\frac{\gamma T_r}{\eta}\right)} . \tag{11}$$

Using the results of equation (11), the model shown in Fig. 9 then becomes that in Fig. 10 for $\omega > \frac{K_{BP}}{\eta}$. The feedback transfer function, H(S), of Fig. 10 may be reduced by algebraic manipulation as shown in Appendix B to equation (12):

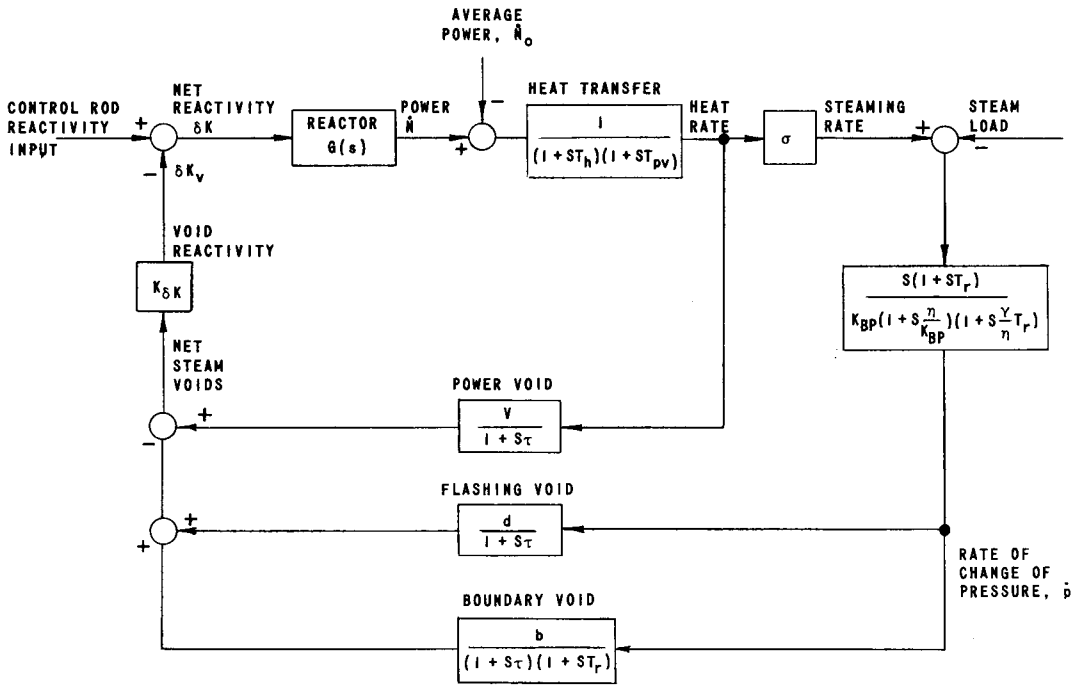

FIG. 9
REACTOR MODEL WITHOUT TEMPERATURE FEEDBACK

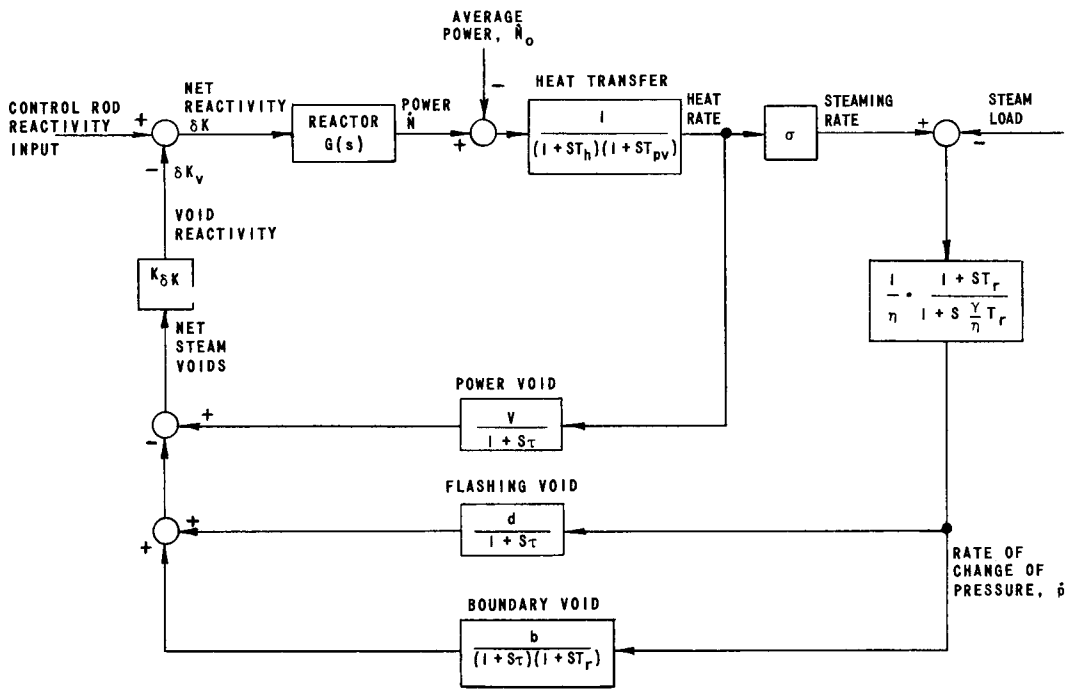

FIG. 10
SIMPLIFIED REACTOR MODEL

$$H(S) = \frac{K_{\delta K}\left[V - \frac{\sigma}{\eta}(b+d)\right]\left[1 + S\left(\frac{(V\gamma - \sigma d)\,T_r}{V\eta - \sigma(b+d)}\right)\right]}{\left(1 + S\frac{\gamma}{\eta}T_r\right)(1 + ST_h)(1 + ST_{pv})(1 + S\tau)} \qquad (12)$$

Figure 11 shows the Bode diagram for equation (12). The shape of this diagram is interesting. Below 0.1 rad/sec the feedback gain is less than that due to the power void reactivity feedback, $K_{\delta K}V$, alone. The reduction is caused by the combined effects of void flashing, d, and void boundary, b, which are pressure dependent. Through the mid-frequency range near 1 rad/sec the feedback amplitude is again less than the power void reactivity feedback, $K_{\delta K}V$, and the reduction is determined by void flashing, d. All pressure effects are absent above about 1 rad/sec, and the reduction of the feedback amplitude at higher frequencies is a function of the fuel heat transfer time constants, T_h and T_{pv}, and of the steam transit time constant, τ. For frequencies greater than $1/\tau$ the feedback amplitude falls off at 18 db/octave.

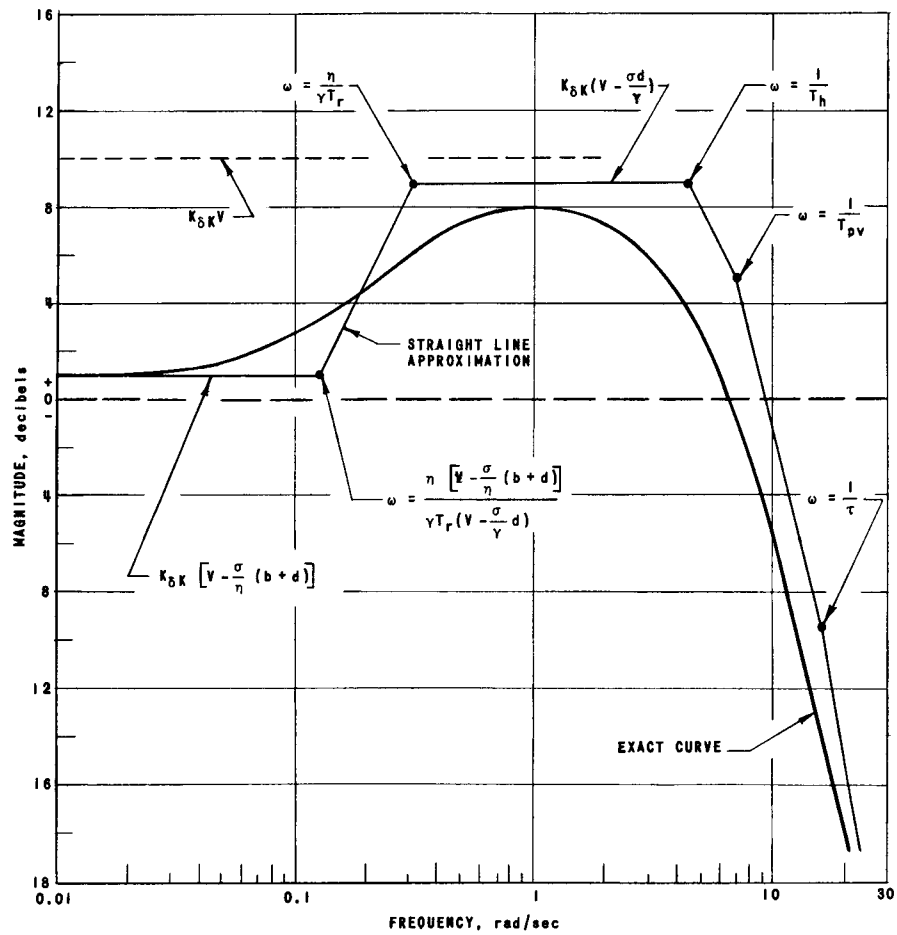

FIG. 11
ANALYTIC BODE FEEDBACK DIAGRAM

IV. DETERMINATION OF POWER COEFFICIENTS AND TIME CONSTANTS

The power coefficients and time constants which describe the reactor can be determined by comparing the amplitude and phase of the experimental feedback transfer function, calculated from the closed loop measurements by the methods of Section II, to the amplitude and phase of the analytic feedback transfer function described by equation (12) of Section III.

Figure 12 shows the analytic feedback response curves obtained

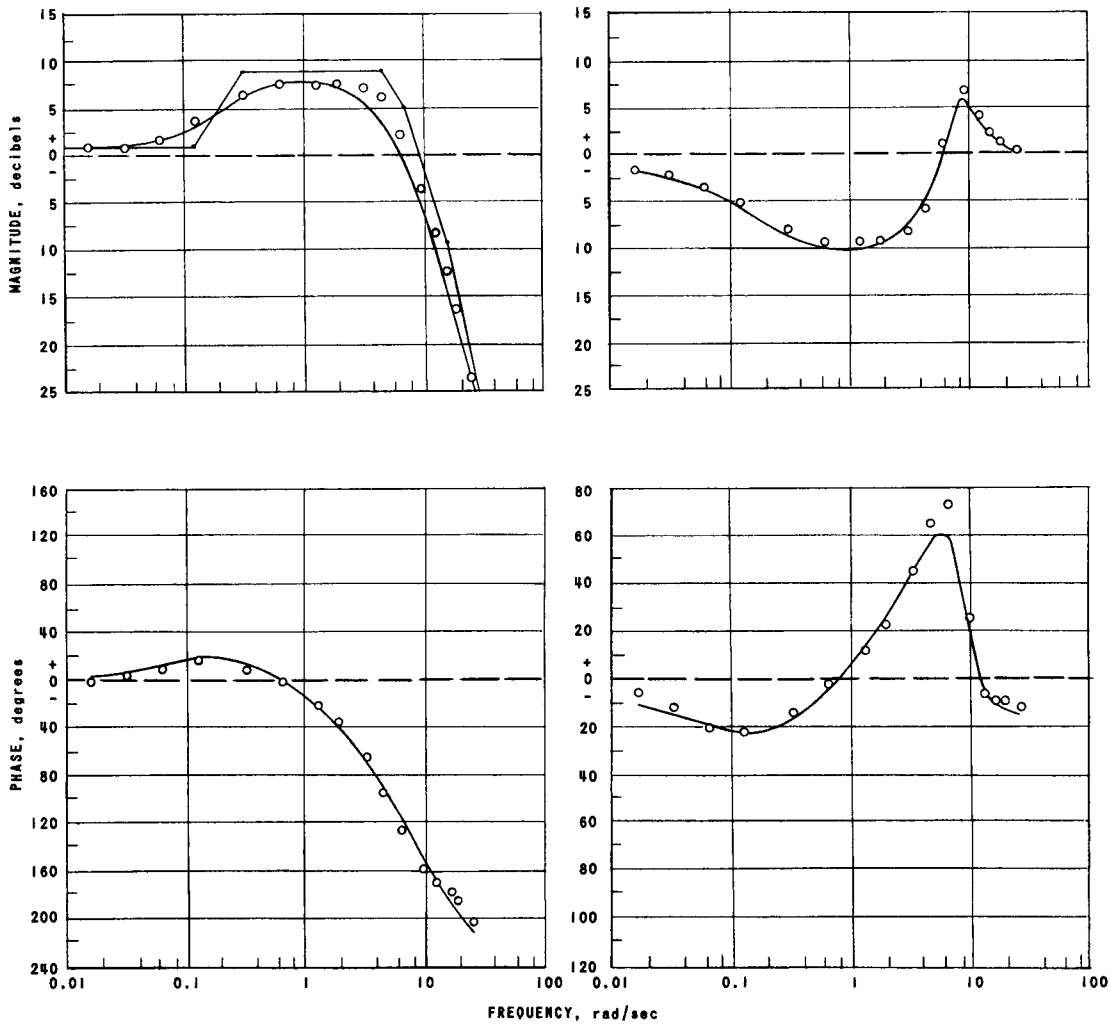

(a) FEEDBACK TRANSFER FUNCTION

(b) POWER TRANSFER FUNCTION

$$H = \frac{1.135(1 + s/0.19)}{(1 + s/0.31)(1 + s/4.4)(1 + s/7)(1 + s/16)}$$

FIG. 12
TRANSFER FUNCTIONS FOR 20 mw, 300 psig

for 20 MW, 300 psi by fitting the experimental data, represented by small circles. The inaccuracy of the fit through the range of 1 to 10 radians/sec is a typical result of lumped-constant representation of a system which possesses distributed constants. Theoretical solutions for the exact representation of the distributed system are currently being investigated.

The analytic expression for Fig. 12 is given by equation (13):

$$H(S) = \frac{1.12\left(1 + \frac{S}{0.12}\right)}{\left(1 + \frac{S}{0.31}\right)\left(1 + \frac{S}{4.4}\right)\left(1 + \frac{S}{7.0}\right)\left(1 + \frac{S}{16}\right)} \quad . \qquad (13)$$

Equation (13) was checked by using it with G(S) to calculate the analytic closed loop frequency response also shown on Fig. 12. The experimental values appear as small circles. The peak analytic phase is less than the experimental phase due to the fact that the feedback transfer function used is a lumped-constant representation of a distributed system.

Equation (13) can be rewritten in the following form:

$$H(S) = \frac{1.12\ (1 + 8.0S)}{(1 + 3.2S)\ (1 + 0.23S)\ (1 + 0.14S)\ (1 + 0.062S)} \quad . \qquad (13a)$$

The power coefficients and time constants in the feedback system can now be readily obtained by comparing equation (13a) with equation (12):

$$K_{\delta K}\left[V - \frac{\sigma}{\eta}(b + d)\right] = 1.12$$

$$\frac{(V\gamma - \sigma\, d)\, T_r}{V\eta - \sigma\,(b + d)} = 8.0$$

$$\frac{\gamma\, T_r}{\eta} = 3.2$$

$$T_h = 0.23 \text{ second}$$
$$\tau = 0.062 \text{ second}$$
$$T_{pv} = 0.14 \text{ second}$$

The static incremental value of 10.1 db for $K_{\delta K}V$ (see Fig. 12) gives:

$$K_{\delta K}V = \text{antilog}_{10}\left(\frac{10.1}{20}\right)$$

$$= 3.2 \quad .$$

The following values are obtained from thermodynamic calculations shown in Appendix C:

γ = 1.08 lb/psi σ = 23 lb/sec

η = 9.32 lb/psi V = 2.2 (ft^3/MW)MW (See Fig. 18)

Then:

$$K_{\delta K} = \frac{3.2}{2.2}$$

$$K_{\delta K} = 1.5 \text{ dollars}/ft^3$$

$$T_r = 3.23\frac{\eta}{\gamma} = \frac{3.23 \times 9.32}{1.08}$$

$$T_r = 28 \text{ seconds}$$

$$d = \frac{1}{\sigma}\left(V\gamma - 8.0 \times 1.12 \times \frac{\eta}{K_{\delta K} T_r} \right)$$

$$d = 0.010 \text{ ft}^3 \text{ sec/psi}$$

$$b = \left(V - \frac{1.12}{K_{\delta K}} \right)\frac{\eta}{\sigma} - d$$

$$b = 0.57 \text{ ft}^3 \text{ sec/psi}$$

The power coefficients and time constants which describe reactor behavior at 20 MW, 300 psig are summarized in Table III.

TABLE III
SUMMARY OF ANALYTIC FEEDBACK PARAMETERS

PARAMETER		TEST NUMBER					
		2	3	4	8	9	10
MW		5.4	9.7	20	5.15	5.1	20
p	psi	550	550	550	300	130	300
γ	lb/psi	1.0	1.0	1.0	1.1	1.1	1.1
η	lb/psi	6.5	6.5	6.5	9.3	15	9.3
σ	lb/sec	6.9	12	26	6.0	5.5	23
V	(ft^3/mw)mw	0.77	1.2	1.5	1.0	1.4	2.2
b	ft^3sec/psi	0.38	0.34	0.19	0.80	2.0	0.57
d	ft^3sec/psi	0.016	0.017	0.010	0.018	0.002	0.010
T_h	sec	0.44	0.38	0.29	0.38	0.31	0.23
T_{pv}	sec	0.22	0.16	0.14	0.17	0.17	0.14
τ	sec	0.084	0.084	0.087	0.083	0.09	0.062
T_r	sec	7.1	12	18	19	24	28
$K_{\delta K}$	\$/ft^3	1.9	1.6	1.8	1.3	1.3	1.5

Figures 13 through 15 are the analytic feedback functions obtained for tests 2, 3, 4, 8, 9 and 14 by the methods described earlier. The corresponding experimental data are shown as small circles on the same figures for comparison purposes. The coefficients and time constants for these curves appear in Table III.

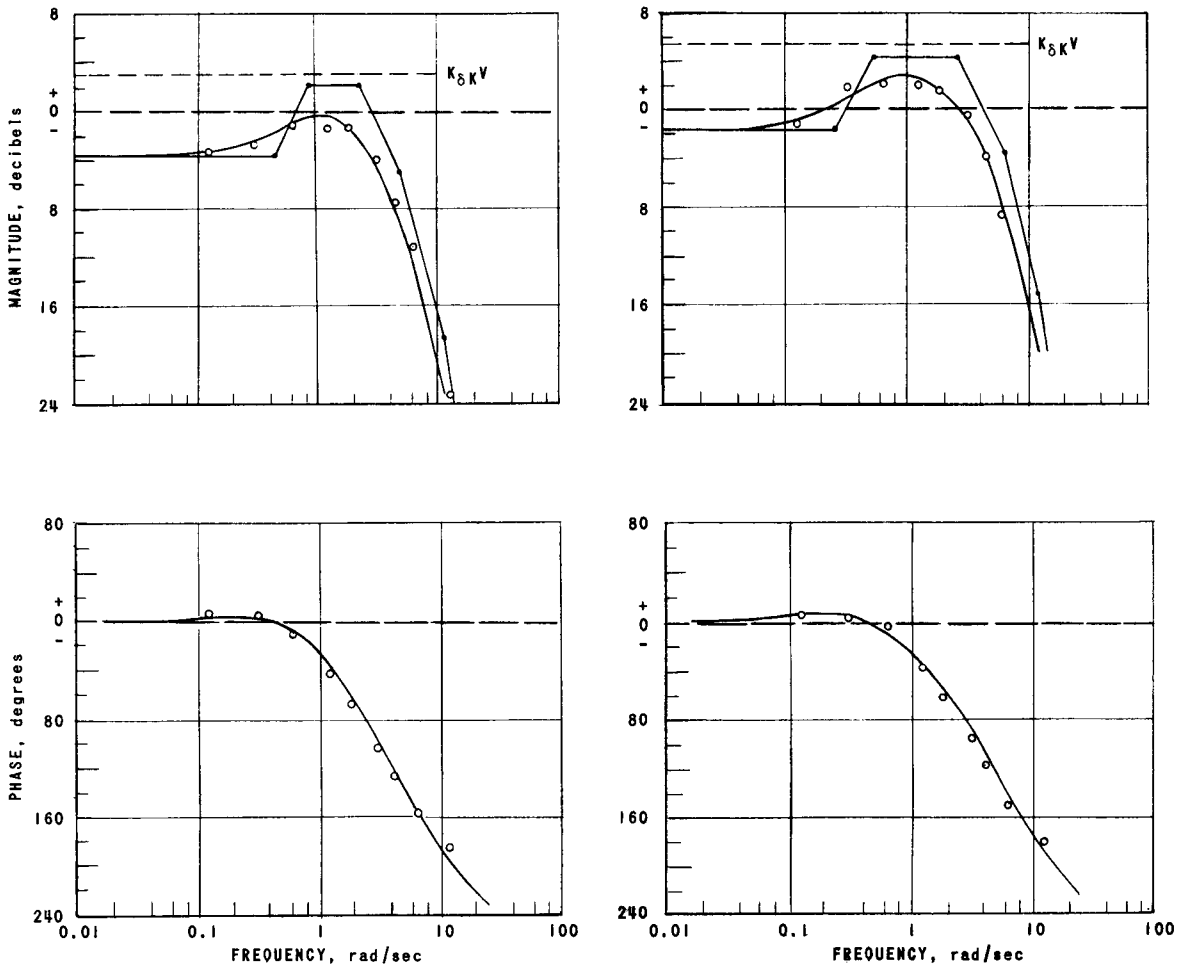

TEST NO. 2: 5.4 mw, 550 psig

$$H(s) = \frac{0.66(1 + s/0.46)}{(1 + s/0.88)(1 + s/2.3)(1 + s/4.3)(1 + s/12)}$$

TEST NO. 3: 9.7 mw, 550 psig

$$H(s) = \frac{0.83(1 + s/0.26)}{(1 + s/0.52)(1 + s/2.6)(1 + s/6.4)(1 + s/12)}$$

FIG. 13
ANALYTIC FEEDBACK FUNCTIONS FOR TESTS 2 AND 3

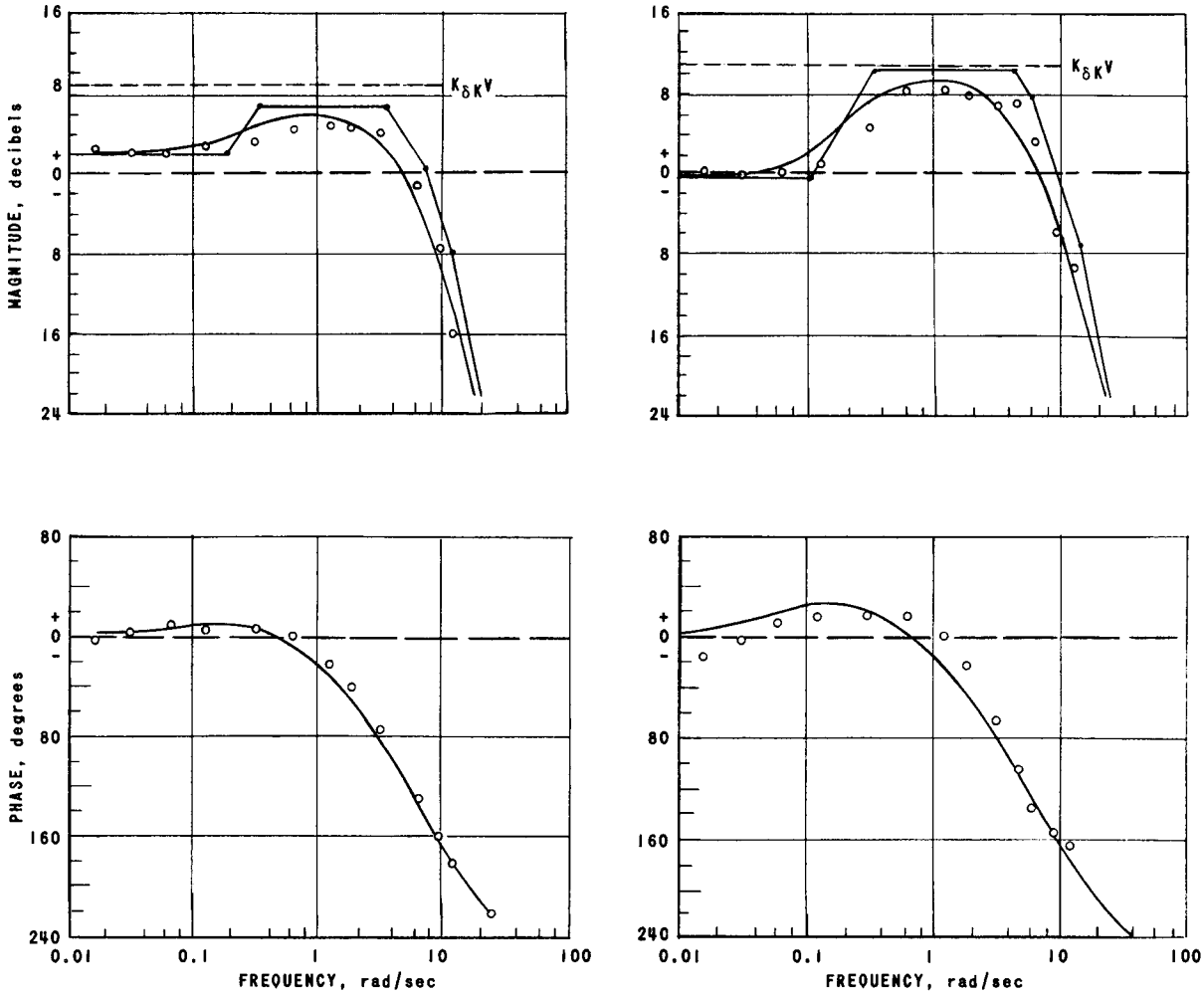

TEST NO. 4: 20 mw, 550 psig

$$H(s) = \frac{1.26(1 + s/0.195)}{(1 + s/0.34)(1 + s/3.5)(1 + s/7)(1 + s/11.5)}$$

TEST NO. 14: 33 mw, 550 psig

$$H(s) = \frac{0.94(1 + s/0.104)}{(1 + s/0.346)(1 + s/4.4)(1 + s/5.9)(1 + s/13.3)}$$

FIG. 14
ANALYTIC FEEDBACK FUNCTIONS FOR TESTS 4 AND 14

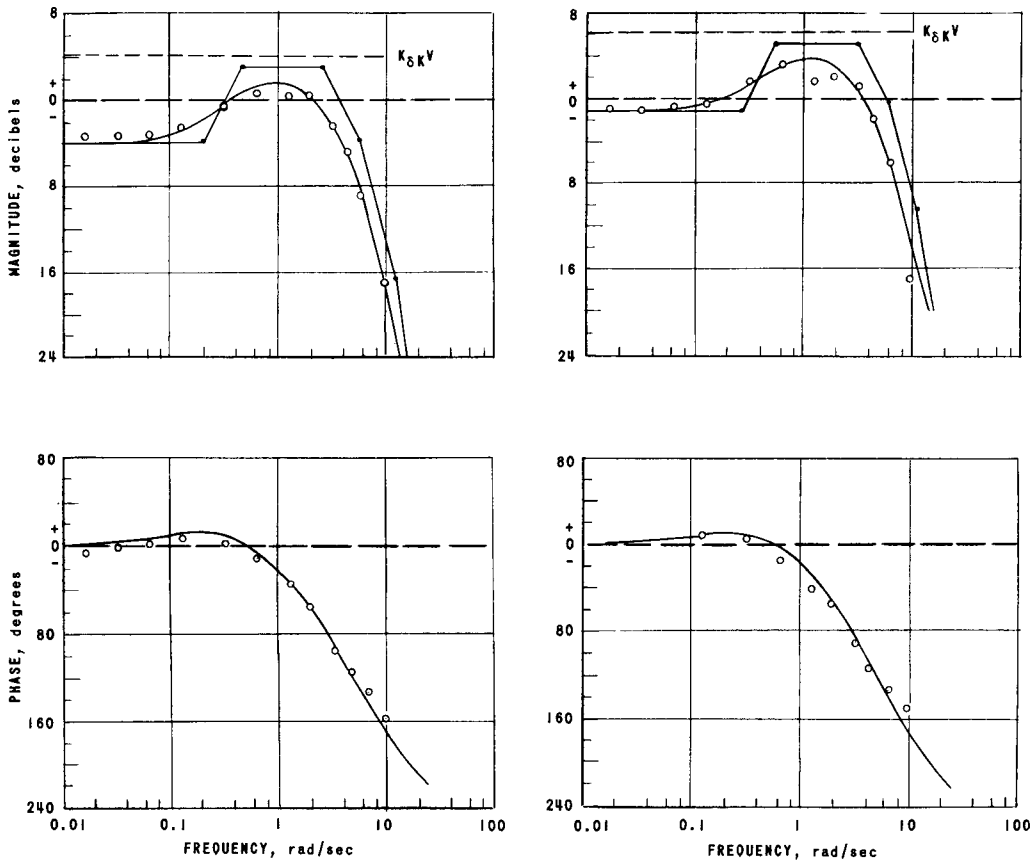

TEST NO. 8: 5.2 mw, 300 psig

$$H(s) = \frac{0.63(1 + s/0.2)}{(1 + s/0.45)(1 + s/2.6)(1 + s/6)(1 + s/12)}$$

TEST NO. 9: 5.1 mw, 130 psig

$$H(s) = \frac{0.87(1 + s/0.27)}{(1 + s/0.56)(1 + s/3.2)(1 + s/6)(1 + s/11)}$$

FIG. 15
ANALYTIC FEEDBACK FUNCTIONS FOR TESTS 8 AND 9

The data from Table III have been plotted in Figs. 16 and 17 with power as the variable and with pressure constant at 550 psig. The curve displaying core total voids (V_0) was calculated from the average void fraction curve given in Fig. 5 of ANL-5607. The measured value of V_0 is 2.5 ft^3 for 7.5% voids.(8) This number was used to normalize Fig. 16 at 20 MW, which corresponds to a steam rate of 60,000 lb/hr on Fig. 5 of ANL-5607. The curve shape otherwise is the same. The power void coefficient (V) was obtained by taking the derivative of (V_0) with respect to power and multiplying it by the power at which the derivative was determined. The small decrease in the void reactivity coefficient ($K_{\delta K}$) with increasing power (as shown in Fig. 16) could be expected since the voids are spreading to lower flux regions where they would have less worth.

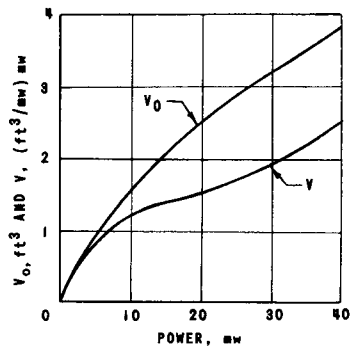

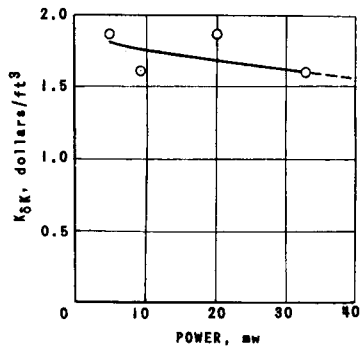

FIG. 16
VARIATION OF POWER COEFFICIENTS
WITH POWER AT 550 psig

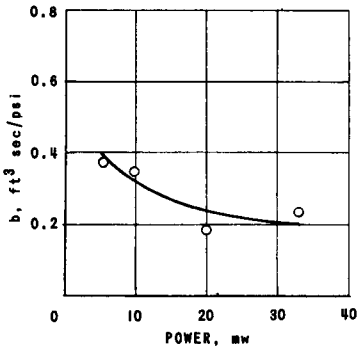

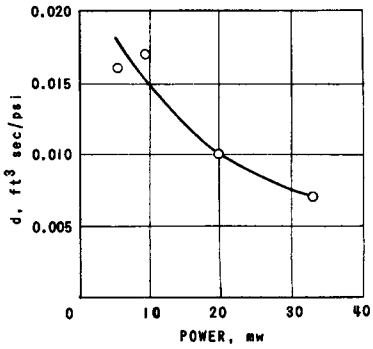

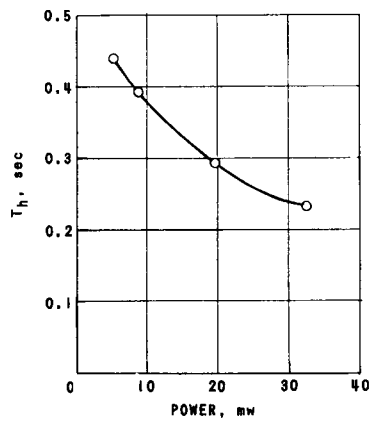

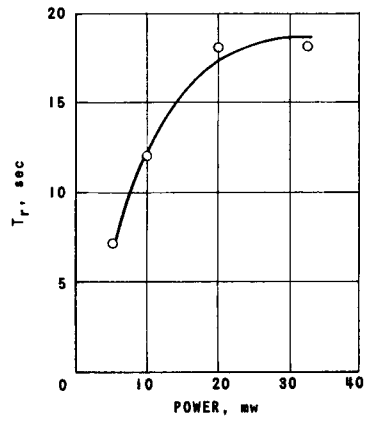

FIG. 17
VARIATION OF TIME CONSTANTS
WITH POWER AT 550 psig

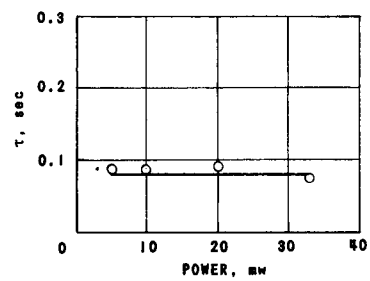

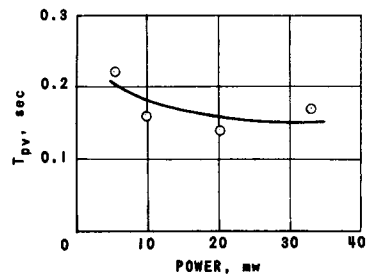

The boundary void coefficient (b) is described by equation (3) in Appendix D, and its variation with power is shown in Fig. 16. The trend is for b to decrease with power while the recirculation time constant (T_r) increases and the steam transit time constant (τ) remains constant, as in Fig. 17. The above conditions appear inconsistent since they require a reduction in the recirculating flow ($\dot{M}_R$) with increasing power. The derivation of equation (3) in Appendix D assumed laminar downcomer flow in the absence of detailed information on actual flow. This assumption may not be justified. Further, the increase in recirculation time constant (T_r) as power increases is not consistent with the increase in recirculation rates indicated by heat balance measurements. Three possible mechanisms which might be responsible are: (1) a convection mixing action in the downcomer; (2) entrainment of steam in the downcomer; (3) a change in flow conditions brought on at some power as a result of the chimney action of the shroud containing the central 36 elements. Investigation is continuing in an effort to improve the model.

The flashing void coefficient (d) is described by equation (1) in Appendix D, and its variation with power is shown in Fig. 16. The decrease in d with power would require a decrease in the mass of water in the boiling portion of the core (M_B), since τ remains constant. This is consistent with the increase in voids that takes place in the boiling region. However, the required decrease in M_B seems larger than might be expected. The large coolant channel width between plates could produce a convection mixing mechanism that would affect M_B and also produce a heat transfer time constant (T_h) which decreases with power as shown in Fig. 17. Inquiries are being directed at the above problem to obtain a better model. The remaining heat transfer time constant (T_{pv}), which is nearly constant with power, has a value which approximates the theoretical value for transfer of heat from the fuel element "meat" to the coolant.

The variations of the above coefficients and time constants with pressure and temperature are shown in Figs. 18 and 19. The curves for power void coefficient (V) were obtained by interpolating the data of Fig. 129 of ANL-5607 to find the V_0 ratio which then was used to ratio V. The void reactivity coefficient ($K_{\delta K}$) increases with temperature in much the same way as does differential rod worth shown in Fig. 13 of reference 8. The effect results from the reduction in water density with increasing temperature.

The trend of the remaining power coefficients and time constants in Figs. 18 and 19 are self-evident. Detailed explanations for their behavior will not be attempted because of the inconsistencies noted above in the discussions of Figs. 16 and 17.

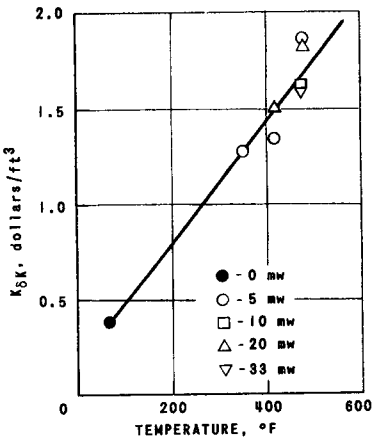

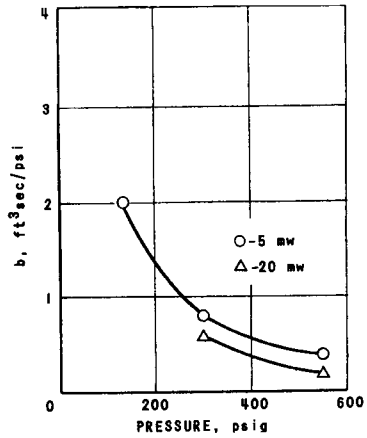

FIG. 18
VARIATION OF POWER COEFFICIENTS WITH PRESSURE AND TEMPERATURE

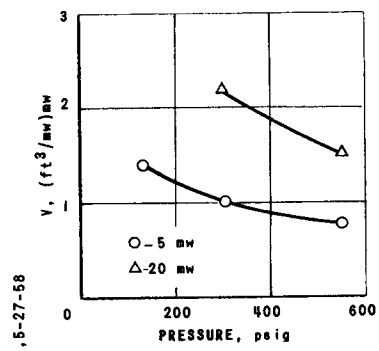

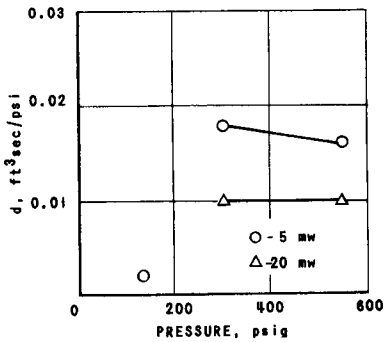

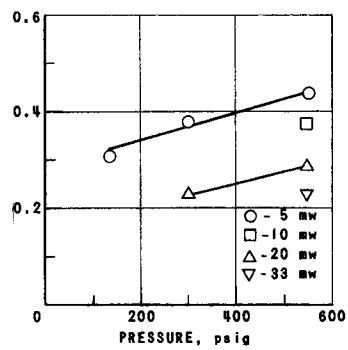

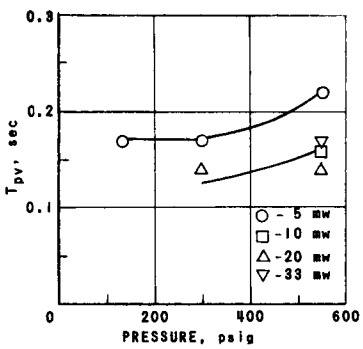

FIG. 19
VARIATION OF TIME CONSTANTS WITH PRESSURE

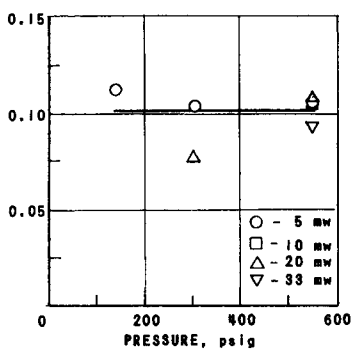

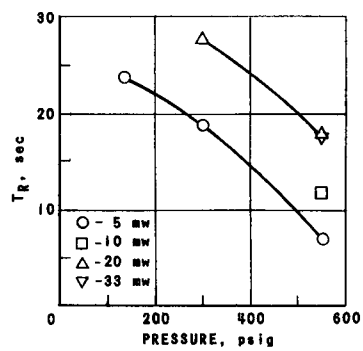

V. EXTRAPOLATION TO HIGHER POWER

Reactor performance and stability may be predicted for power levels well in excess of those for which dynamic measurements exist. A power transfer function may be calculated and stability determined by measuring the reactivity feedback function at low power and then extrapolating it to the desired power. In the case of boiling reactors, reduced pressure tests provide a convenient means for accomplishing this. A pressure reduction to one-half normal increases the steam void volume to correspond roughly with that produced by doubling power. The transfer function measured under reduced pressure conditions therefore provides values for the time constants associated with heat transfer, steam transit, and water recirculation as they would exist if power were increased by the appropriate amount. The value of $K_{\delta K}V$ may also be obtained during the reduced pressure test by a static measurement made while holding reactor pressure constant at the test value. $K_{\delta K}V$ is important to reactor stability since it determines the gain magnitudes for both the feedback and the open loop transfer functions. In general, a reduction of $K_{\delta K}V$ will result in improved stability by virtue of the increase in gain margin that occurs if all time constants remain unchanged. The value of $K_{\delta K}V$ may also be obtained by measuring the reactivity-in-voids vs. power curve for the pressure to be used at the higher power condition and then extrapolating to the desired power. Such a curve is shown in Figure 20.

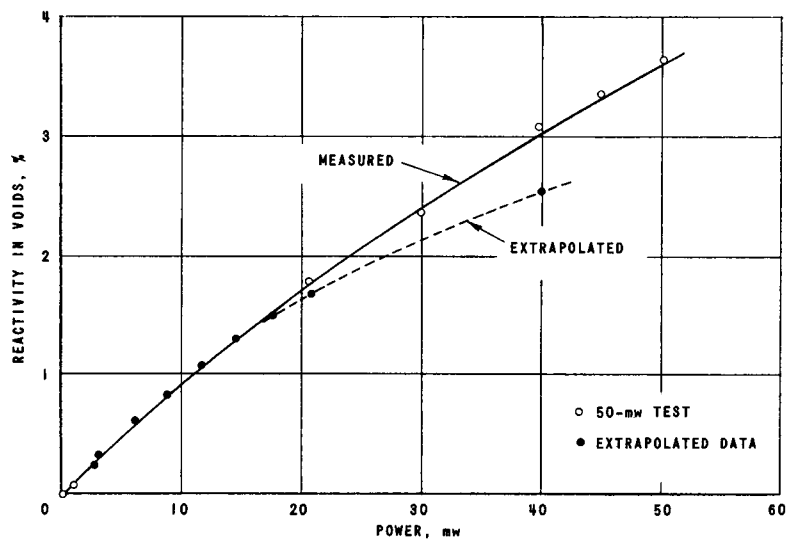

FIG. 20
REACTIVITY IN VOIDS AS A FUNCTION OF POWER

The ordinate is defined as the excess reactivity that would exist if the voids were suddenly removed with all other conditions remaining constant. It is expressed in terms of a hot non-boiling rod calibration. In the actual case the rod calibration is strongly affected by the steam void content of

the core, so $K_{\delta K}V$ is determined by taking the ratio of the slope at the high power to that at low power and multiplying by the value of $K_{\delta K}V$ obtained from the transfer function measurement made at the low power. The actual void reactivity curve measured later is also shown on Fig. 20. The extrapolated value at 40 MW is within about 16% of the actual value.

The two constant-gain asymptotes required in addition to $K_{\delta K}V$ to determine the new high-power feedback function must be obtained by extrapolation of the coefficients determined for the low power normal pressure condition. Coefficients γ, η, and σ are dependent upon operating pressure only and may be calculated directly using data obtained from steam tables, as indicated in Appendix C.

The power steam void coefficient, V, may be extrapolated with reasonable accuracy by calculations using two-phase heat transfer data obtained from electrically heated boiling loops[10] (see Fig. 16 and Appendix D). The boundary and flashing coefficients determined from the low power transfer function may be extrapolated by evaluating the theoretical expressions utilizing the data obtained from the reduced pressure experiment. Appendix D presents calculations made to extrapolate from 20 MW to 40 MW at 550 psig. Use was made of the data in Section IV for 20 MW at 300 psig. The H function predicted for 40-MW operation as a result of these calculations is

$$H = \frac{1.35\ (1 + 10.8S)}{(1 + 0.062S)\ (1 + 0.14S)\ (1 + 0.23S)\ (1 + 4.5S)} \quad . \tag{14}$$

The predicted power transfer function for 40 MW, obtained by combining equation (14) with G, the zero power function, is shown in Fig. 21 which displays both amplitude and phase response. Experimental points determined during a subsequent run made at 33 MW are shown as small circles on the same figure. The dashed curve is the analytical curve representing these points. The analytic 33-MW feedback function used to obtain the dash curve was

$$H = \frac{0.94\ (1 + 9.6S)}{(1 + 0.075S)\ (1 + 0.17S)\ (1 + 0.23S)\ (1 + 2.9S)} \quad . \tag{15}$$

Amplitude and phase curves for Equation (15) are plotted on Fig. 14.

It was necessary to run at 33 MW rather than 40, because the excess reactivity of the reactor was insufficient to reach the 40-MW level and still maintain equilibrium xenon. The powers are sufficiently close,

---

[10] "The Experimental Boiling Water Reactor," ANL-5607 (May, 1957)

however, to permit comparison of the data, since small differences in power do not produce drastic changes in the curve. The largest error in the prediction occurs in the low-frequency region which is sensitive to power level change due to the influence of V and b.

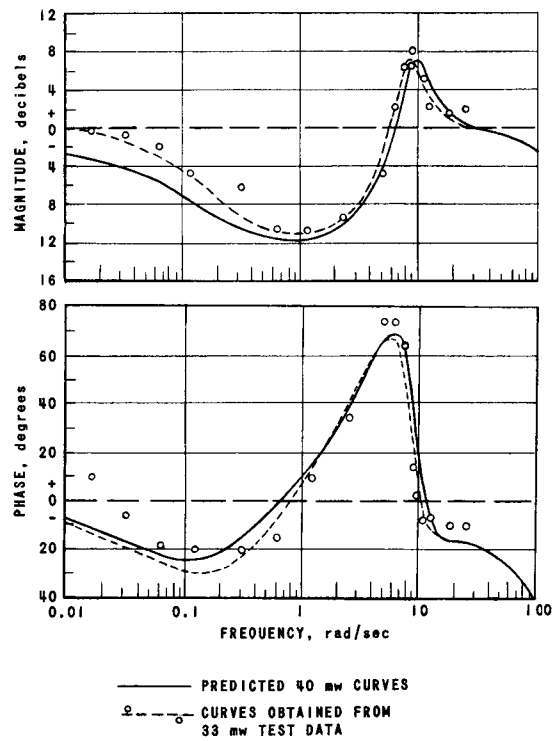

FIG. 21
PREDICTED 40 mw POWER TRANSFER FUNCTION

Table IV summarizes the gain coefficients and time constants for the 40-MW predicted analytic H function and for the 33-MW analytic H function determined from experiment. The value of the boundary coefficient, b, is higher at 33 MW than at 40 MW, as would be expected for a lower power. The flashing coefficient, d, theoretically would decrease with power as shown. T_h, T_{pv} and τ all compare favorably. T_r is considerably in error. A better estimate of this quantity could have been obtained from the information presented in Table III if it had been available in time. For example, T_r shows considerable decrease as pressure is raised. Also, since power was at 33 MW rather than at 40 MW, a smaller value would be expected, applying the trends of Table III. The estimate of $K_{\delta K}$ was in error by about 10%. Again, a better value could have been estimated if Table III had been available. It is recommended that all measured data be processed before prediction, if possible, to establish trends and improve extrapolation.

TABLE IV

COMPARISON OF PREDICTED AND EXPERIMENTAL FEEDBACK PARAMETERS

	40-MW Extrapolation	33-MW Test
Power-MW	40	33
Pressure - psig	550	550
γ - lb/psi	1.05	1.05
η - lb/psi	6.53	6.53
σ - lb/sec	51.2	42
V - ft^3	2.6	2.1
b - ft^3 sec/psi	0.20	0.23
d - ft^3 sec/psi	0.004	0.007
T_h - sec	0.23	0.23
T_{pv} - sec	0.14	0.17
τ - sec	0.062	0.075
T_r - sec	28	18
$K_{\delta K}$ - \$/ft^3	1.4	1.6

VI. INVESTIGATION OF OSCILLATION THRESHOLD

The reactor would be stable for all values of open loop gain if no time lags were present in the reactivity feedback. In the actual case, there are several time lags associated with the feedback which result in increased phase shift at higher frequencies. This is shown in Fig. 22, which is a log polar plane plot of the frequency locus of the open loop transfer function, GH, for the 20 MW, 550 psig experiment designated as test #4 in Table I. The point of interest is the magnitude of the open loop gain when the open loop phase shift is -180 degrees. At -180 degrees phase shift, the equation describing the closed loop power transfer function, P, can be written:

$$|P| = \frac{|G|}{1 - |GH|} \quad . \tag{16}$$

As $|GH|$ becomes unity, $|P|$ will approach infinity and the reactor flux will oscillate weakly at a frequency very nearly equal to the frequency for which $|P|$ is infinite.

Gain margin is a term used to designate stability in quantitative terms. It is defined as the increase in gain that will produce unity open loop gain at -180 degrees shift. In Fig. 22, the margin is $1/0.22$, where 0.22 is equivalent to the -180° curve intercept of -13.1 decibels. It is convenient to plot the absolute magnitude of GH that exists at -180° rather than its reciprocal, which is the gain margin. This is shown in Fig. 23 where oscillation will occur when the ordinate is unity or larger as indicated by the region marked "unstable operation."

The 33-MW experiment discussed in Section V indicated large gain and phase margins existed at that power, so a 50-MW test was made. Two additional points were obtained for Fig. 23, using 33 and 50 MW data and the method of Fig. 22. An extrapolation of these results indicated the onset of instability at a power level of about 66 MW. A check was provided by also evaluating phase margin, which is defined as the amount of additional phase lag required to produce 180 degrees lag when added to the open loop phase shift that exists at unity gain or zero decibels on Fig. 22. This again is the condition for complete oscillatory instability. The phase margins for 5, 20, and 50 MW are plotted on Fig. 23. Extrapolation to zero-phase margin shows that instability occurs at about 66 MW, as was the case for the gain margin extrapolation.

A system exhibits resonance peaking in the frequency domain as the gain and phase margins approach unity and zero, respectively. The underdamped condition represented by the above appears in the time domain as a decaying oscillatory response to step inputs. For this reason

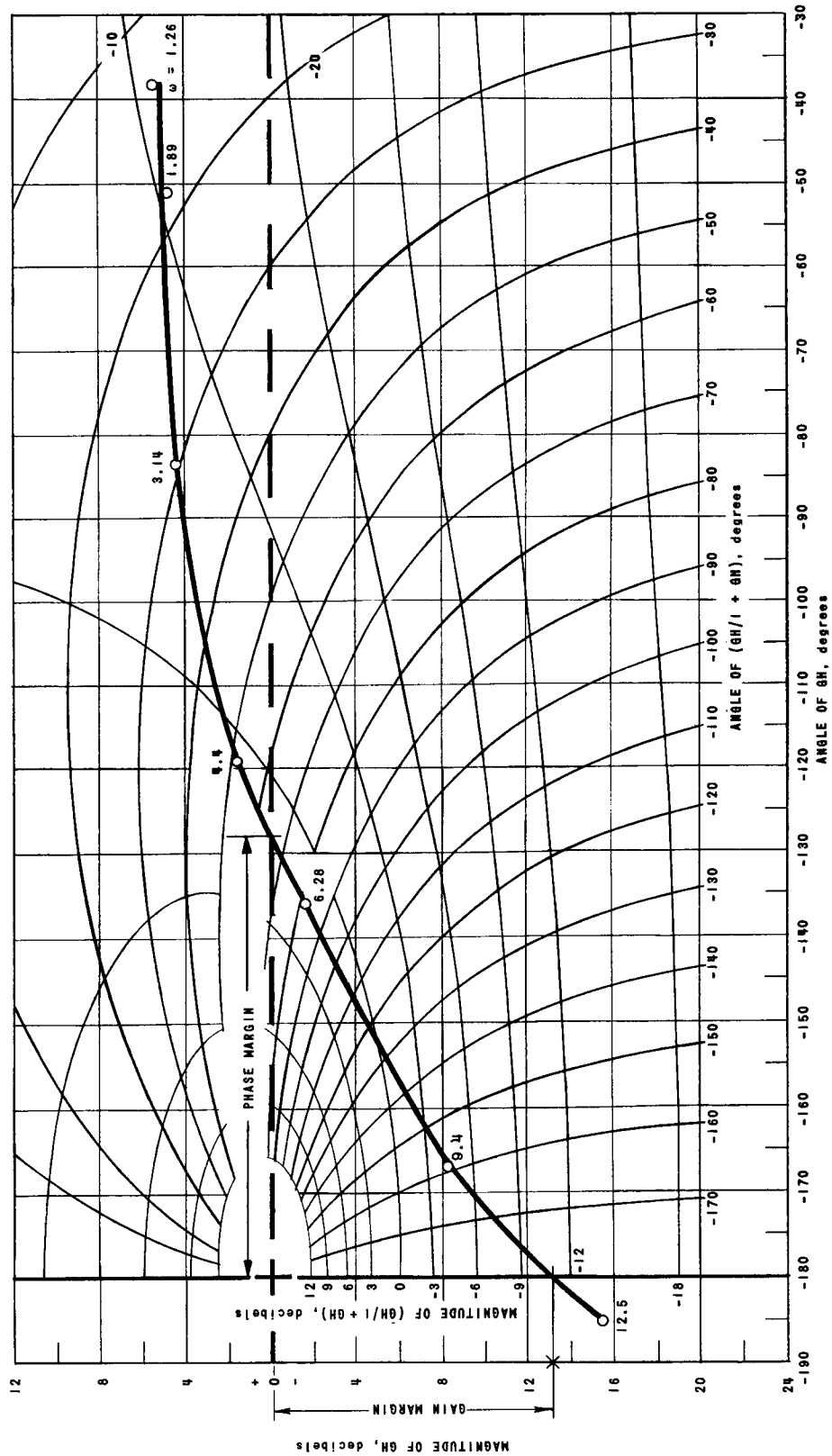

FIG. 22
OPEN LOOP FREQUENCY LOCUS FROM TEST NO. 4

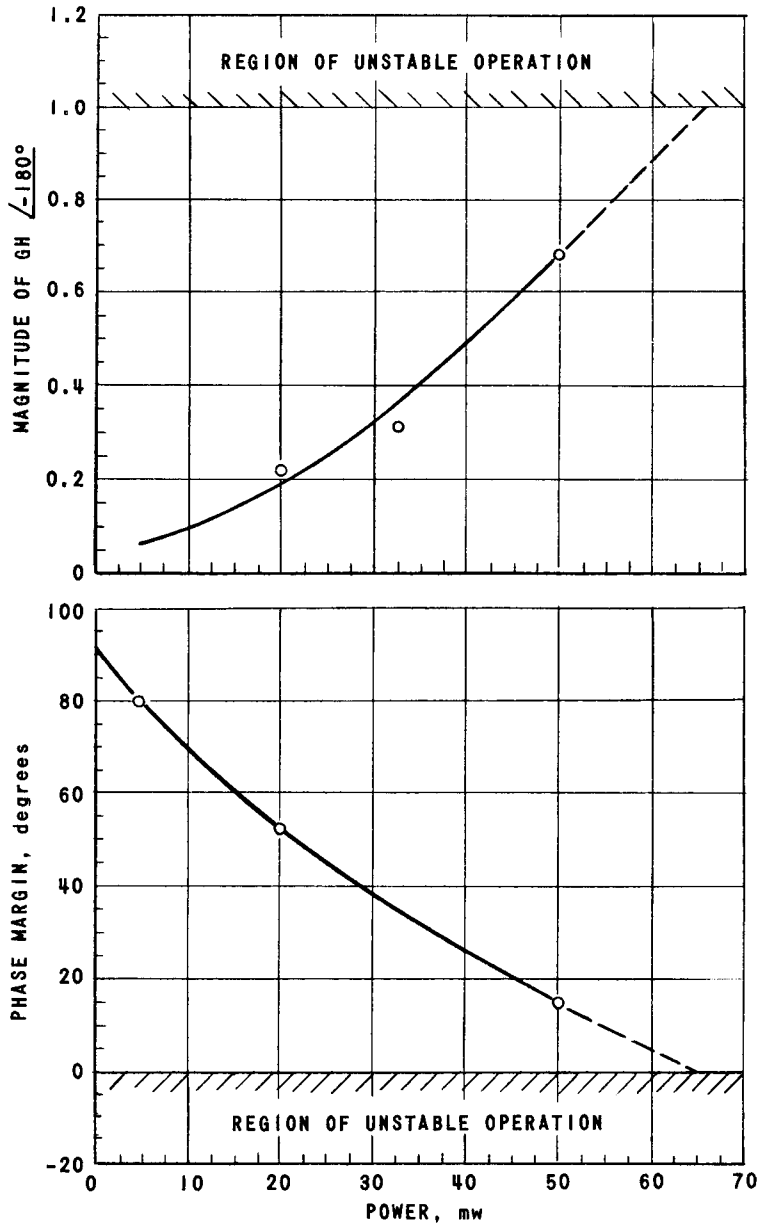

FIG. 23
REACTOR GAIN AND PHASE STABILITY

a series of step-reactivity flux responses were measured during the probing run to 50 MW. Fig. 24 shows the reactivity input and flux response for 18, 30 and 40 MW, respectively. Reactivity is proportional to rod position displayed by the bottom trace. Flux response to the reactivity insertion is shown full scale in the top trace and to an expanded scale in the center trace.

The rate of decay of the oscillatory flux response is very rapid at 18 MW, where the gain margin is 5 and the phase margin is 50 degrees. On the other hand, the decay requires many cycles at 40 MW, where the gain margin of 2 and the phase margin of 25 degrees represent a much lower degree of damping. The step method is therefore a means for gross observation of the approach to instability. Reactivity boiling noise limits the usefulness of the method by causing considerable flux noise in the frequency region corresponding to the frequency of the decaying flux transient. Another practical limit is the difficulty of producing a reactivity step of sufficient magnitude and short enough rise time with conventional power-reactor control rod drives. The above recordings show rise times of about 140 milliseconds for the two-inch rod displacement. This motion represents about 0.08% reactivity change and was obtained by adapting the transfer function drive. Even with this drive, EBWR ran out of reactivity, and it was not possible to obtain sufficient reactivity input to take meaningful step data above the 40-MW point.

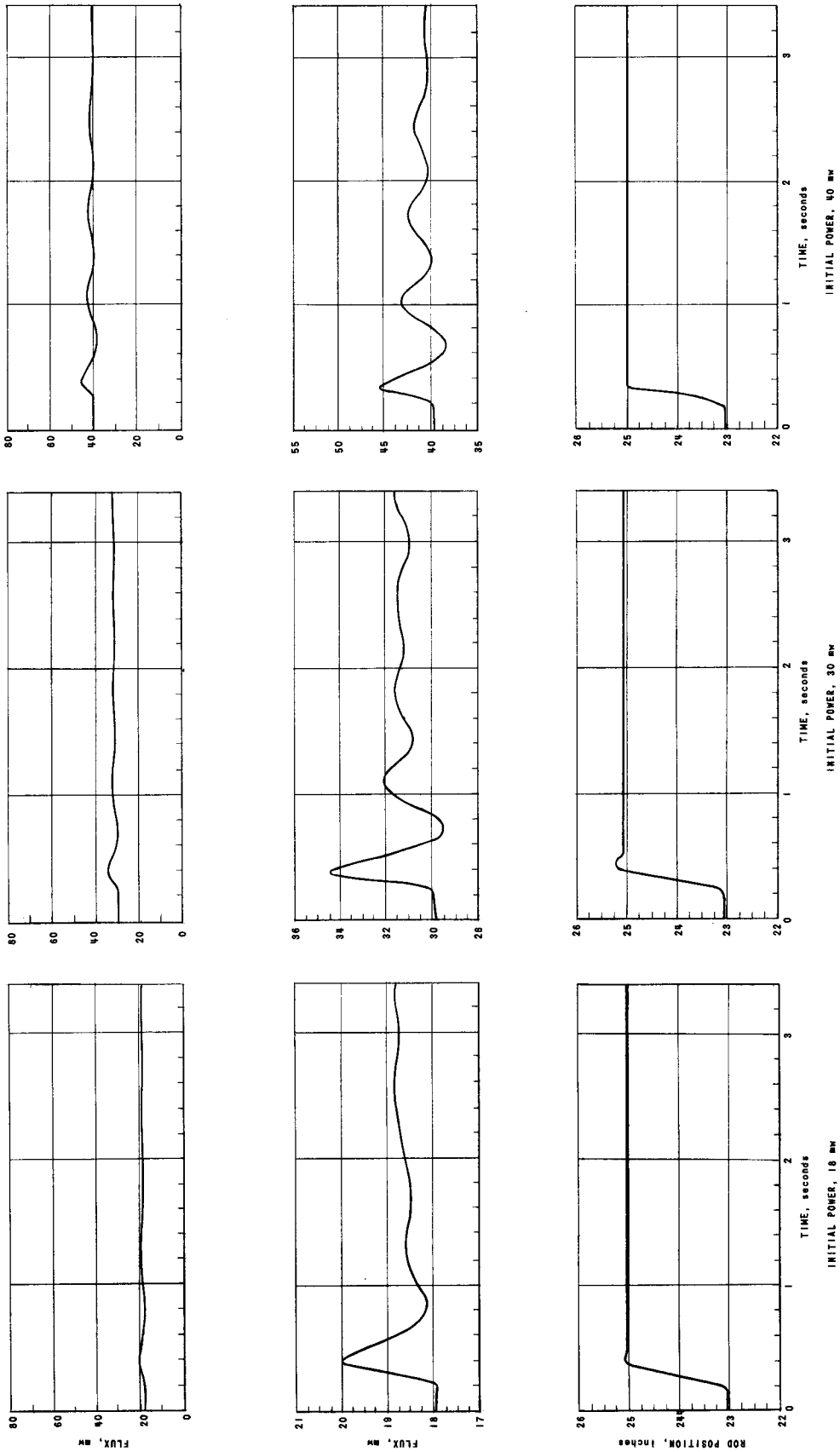

FIG. 24
FLUX RESPONSE TO A REACTIVITY STEP FOR VARIOUS POWERS AT 600 psig

VII. CONCLUSIONS

Another high-power experiment was performed subsequent to the 50-MW test to determine whether the reactor was stable up to the 66-MW threshold determined in Section VI. At 61.7 MW, feedwater pump capacity was reached. Power was increased in short bursts to an estimated 65 MW with reactor water level falling slightly. The reactor remained stable and controllable. The flux record produced by a fast oscillograph exhibited large amplitude building and decaying oscillatory wave trains, 6 to 7 cycles in length, which were excited by reactivity boiling noise. The results of the transient tests discussed in Section VI, coupled with the above observations, suggest that the phase margin had been reduced to about 5 degrees or less and that loss of reactor control could occur at a power level not far above the 65 MW attained in the above test.

The feedback loop gain, $K_{\delta K}V$, is a very important stability criteria since it sets the gain margin. It is defined as the operating power in MW times the slope of the void-reactivity vs. power curve measured at operating power. The normalized G function gain is unity so the total loop gain is numerically equal to $K_{\delta K}V$. Figure 25 shows $K_{\delta K}V$ versus power and the power coefficient of reactivity, $(K_{\delta K}V)/MW$ versus power. The decrease in the power coefficient with increasing power occurs because the voids/MW coefficient, V/MW, decreases with power as does the reactivity worth/unit void coefficient, $K_{\delta K}$.(10,11) The significance here is the possibility of designing a core whose void coefficient decreases even more rapidly with power than shown above. The open loop gain

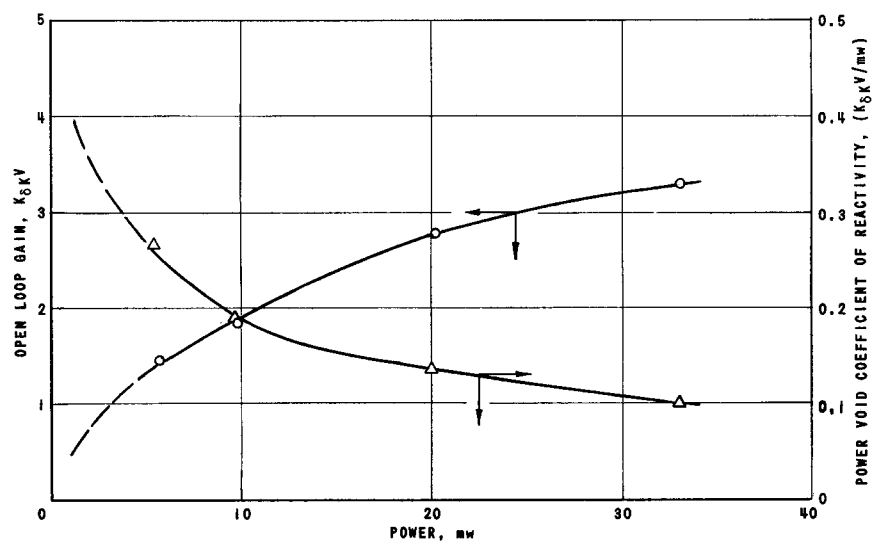

FIG. 25
VOID COEFFICIENT OF REACTIVITY

[11] J. A. DeShong, Jr. "Styrofoam Simulation of Boiling and Temperature Effects in the EBWR Cold Critical Experiments," ANL-5697, (May, 1957).

would reach a peak value and then start decreasing. Once reactor power goes beyond the value at which maximum loop gain occurs, stability will improve provided the important feedback time constants continue to decrease. Unless some unforeseen effect, e.g., a hydraulic resonance, made its appearance, power could be increased to the burnout point in such a design.

The techniques used herein for stability analysis of a particular plant may be extended to variable parameter studies to obtain improved core designs. One such study was made to determine the effect of the heat transfer time constant magnitude on stability, assuming that T_{pv} and τ remain constant. (It is conceivable that T_{pv} might also vary in some portion to T_h, which would, of course, alter the results.) The curves obtained in the study are shown in Fig. 26, which shows P function gain and phase, respectively. The reference curve, labeled (5), is the

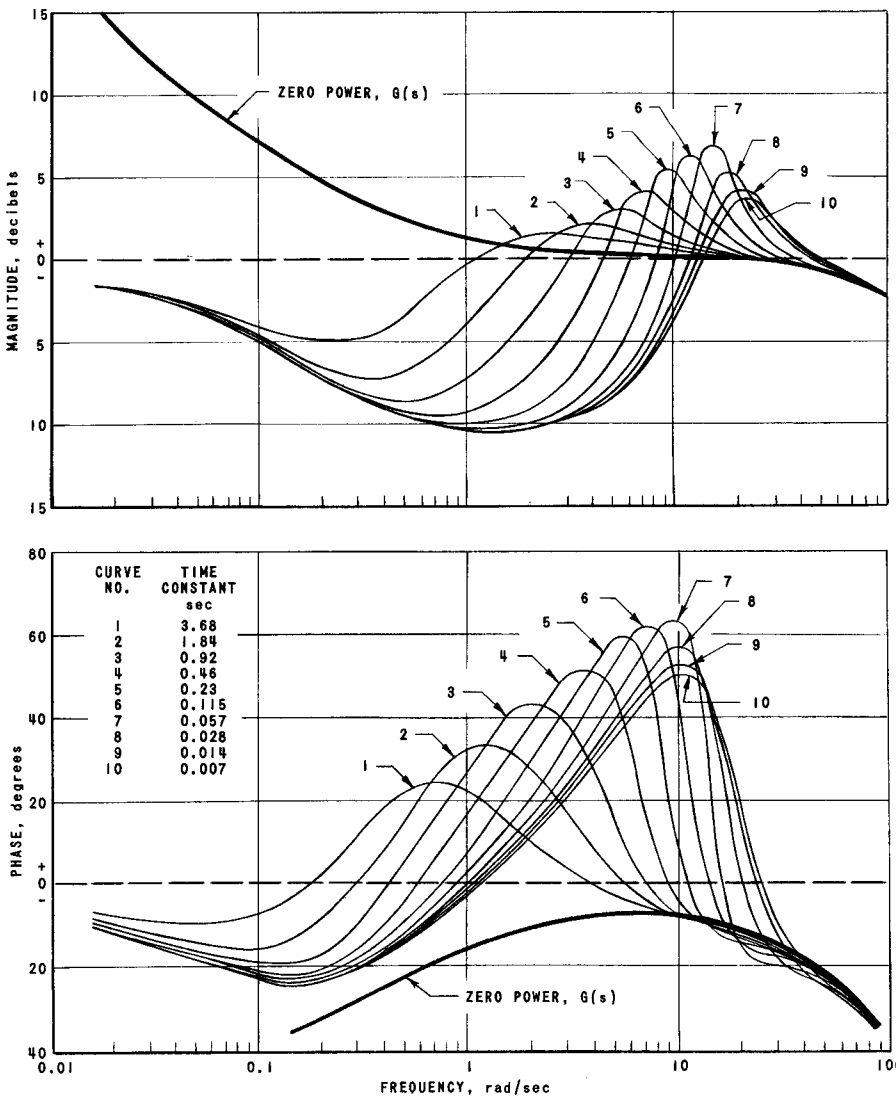

FIG. 26
HEAT TRANSFER STABILITY STUDY

20 MW, 300 psig test #10 of Table I. T_h was varied by multiple factors of 2 from the reference test value of 0.23 second as shown. Note that the curve indicating least stability occurs for a value of T_h about one-fourth of the reference value. However, as T_h is decreased further toward the very short time constants encountered in the early BORAX reactor fuel elements, the resonance peak magnitude decreases, indicating better stability.

Reactor stability is markedly improved by a large increase in T_h, as shown by curve (1) representing a 16X increase. Fuel elements of this type could be produced by employing a gas filling for heat conduction from the meat to an unbonded clad, as compared to the more usual methods employing either a fluid heat conducting medium such as sodium or an intermetallic bond between clad and meat. The gas method would be accompanied by higher internal fuel temperatures, and the self-limiting expulsion of water from the core on accidental power excursions would be delayed.

Experimental measurements to be used for analyses of the type described herein must be very precise to obtain the desired results. Accuracy of $\pm$ 1% and $\pm$ 1 degree in the presence of a signal-to-noise ratio of 2/1 would be desirable where a system with the same degree of complexity as the boiling reactor is being analyzed.

ACKNOWLEDGMENTS

The authors gratefully acknowledge the contributions of Alex Gerba, Jr., Louis Palacios, and Raymond Viskanta who calculated many of the analytic feedback functions and much of the data in Table III. J. M. Harrer contributed many valuable suggestions as did P. A. Lottes who was consulted on heat transfer problems and J. A. Thie who was consulted on physics problems.

APPENDIX A

CALCULATION OF PRESSURE TRANSFER FUNCTION

Reference (1) established the following relationship:

$$\dot{p}(j\omega)\left\{\frac{m_1}{p} - \frac{m_1}{\theta}\frac{\partial\theta}{p} + \frac{m_1\dfrac{\partial h_s}{\partial p}}{h_s - h_w} + \frac{\dfrac{\partial h_w}{\partial p}}{h_s - h_w}\left[M_B + \left(1 - \frac{1}{r_r}\right)\left(M_{NB}\, e^{-j\omega T_r}\right) + (M - M_c)\, F(j\omega)\right]\right\}$$

$$= \frac{\dot{N}(j\omega)}{h_s - h_w} - \dot{m}_2(j\omega) - \left(\frac{h_w - h_{FW}}{h_s - h_w}\right)\dot{M}_{FW}(j\omega) \quad . \qquad (1)$$

Equation (1) can be simplified by using the following approximation:

$$\left[M_B + \left(1 - \frac{1}{r_r}\right)\left(M_{NB}\, e^{-j\omega T_r}\right) + (M - M_c)\, F(j\omega)\right] \approx \frac{M}{1 + j\omega T_r} \quad . \qquad (2)$$

Using the approximation of equation (2), equation (1) becomes:

$$\dot{p}(j\omega)\left\{\frac{m_1}{p} - \frac{m_1}{\theta}\frac{\partial\theta}{\partial p} + \frac{m_1\dfrac{\partial h_s}{\partial p}}{h_s - h_w} + \left(\frac{\dfrac{\partial h_w}{\partial p}}{h_s - h_w}\right)\left(\frac{M}{1 + j\omega T_r}\right)\right\}$$

$$= \frac{\dot{N}(j\omega)}{h_s - h_w} - \dot{m}_2(j\omega) - \left(\frac{h_w - h_{FW}}{h_s - h_w}\right)\left(\dot{M}_{FW}(j\omega)\right) \quad . \qquad (3)$$

To facilitate further manipulation of equation (3), the following definitions are used:

$$\gamma = \frac{m_1}{p} - \frac{m_1}{\theta}\frac{\partial\theta}{\partial p} + \frac{m_1\dfrac{\partial h_s}{\partial p}}{h_s - h_w} \quad ; \qquad (4)$$

$$\eta = \frac{m_1}{p} - \frac{m_1}{\theta}\frac{\partial\theta}{\partial p} + \frac{m_1\dfrac{\partial h_s}{\partial p}}{h_s - h_w} + \frac{M\dfrac{\partial h_w}{\partial p}}{h_s - h_w} \quad . \qquad (5)$$

Substituting equations (4) and (5) into equation (3) gives

$$\dot{p}(j\omega)\left\{\gamma + \frac{(\eta - \gamma)}{1 + j\omega T_r}\right\} = \frac{\dot{N}(j\omega)}{h_s - h_w} - \dot{m}_2(j\omega) - \left(\frac{h_w - h_{FW}}{h_s - h_w}\right)\left(\dot{M}_{FW}(j\omega)\right) \quad . \qquad (6)$$

Using transfer function notation, equation (6) gives

$$\frac{\dot{p}(S)}{\frac{\dot{N}(S)}{h_s - h_w} - \dot{m}_2(S) - \left(\frac{h_w - h_{FW}}{h_s - h_w}\right) \dot{M}_{FW}(S)} = \frac{1}{\gamma + \frac{\eta - \gamma}{1 + ST_r}} \quad . \tag{7}$$

The right hand side of equation (7) can be simplified:

$$\frac{\dot{p}(S)}{\frac{\dot{N}(S)}{h_s - h_w} - \dot{m}_2(S) - \left(\frac{h_w - h_{FW}}{h_s - h_w}\right) \dot{M}_{FW}(S)} = \frac{1 + S\,T_r}{\eta\left(1 + S\,\frac{\gamma}{\eta}\,T_r\right)} \quad . \tag{8}$$

The denominator of the left-hand side of equation (8) represents the rate of change of mass in the reactor vessel; therefore the right hand side of equation (8) gives the transfer function for rate of change of pressure with respect to rate of change of mass. Equation (8) represents the forward portion of the minor loop shown in Fig. 8.

APPENDIX B

CALCULATION OF FEEDBACK TRANSFER FUNCTIONS FOR FIGURES 9 AND 10

$$\frac{\delta K_v}{\dot{N}}(S) = \left(\frac{1}{(1 + ST_h)(1 + ST_{pv})}\right)\left\{\frac{V}{1 + S\tau} - \left[\frac{S(1 + ST_r)\sigma}{K_{BP}\left(1 + S\frac{\eta}{K_{BP}}\right)\left(1 + S\frac{\gamma}{\eta}T_r\right)}\right]\left[\frac{d}{1 + S\tau} + \frac{b}{(1 + S\tau)(1 + ST_r)}\right]\right\} K\delta K \tag{1}$$

$$\frac{\delta K_v}{\dot{N}}(S) = \left(\frac{K_{\delta K}}{(1 + ST_h)(1 + ST_{pv})}\right)\left\{\frac{V}{1 + S\tau} - \left[\frac{S\sigma(1 + S\,T_r)}{K_{BP}\left(1 + S\frac{\eta}{K_{BP}}\right)\left(1 + S\frac{\gamma}{\eta}T_r\right)}\right]\left[\frac{d + S\,d\,T_r + b}{(1 + S\tau)(1 + ST_r)}\right]\right\} \tag{2}$$

$$\frac{\delta K_v}{\dot{N}}(S) = \left(\frac{K_{\delta K}}{(1 + ST_h)(1 + ST_{pv})}\right)\left\{\frac{V}{1 + S\tau} - \frac{S\sigma(b + d + S\,d\,T_r)}{K_{BP}\left(1 + S\frac{\eta}{K_{BP}}\right)\left(1 + S\frac{\gamma}{\eta}T_r\right)(1 + S\tau)}\right\} \tag{3}$$

$$\frac{\delta K_v}{\dot{N}}(S) = \left(\frac{K_{\delta K}}{(1 + ST_h)(1 + ST_{pv})}\right)\left\{\frac{VK_{BP} + S\,V\,K_{BP}\left(\frac{\eta}{K_{BP}} + \frac{\gamma}{\eta}T_r\right) + S^2\,V\,\gamma\,T_r + S\sigma(b + d) - S^2\sigma d T_r}{K_{BP}\left(1 + S\frac{\eta}{K_{BP}}\right)\left(1 + S\frac{\gamma}{\eta}T_r\right)(1 + S\tau)}\right\} \tag{4}$$

$$\frac{\delta K_v}{\dot{N}}(S) = \frac{K_{\delta K}\left[S^2 T_r (V\gamma - \sigma d) + S\left(V\eta - V\frac{\gamma}{\eta}T_r K_{BP} + \sigma b + \sigma d\right) + V K_{BP}\right]}{K_{BP}(1 + ST_h)(1 + ST_{pv})\left(1 + S\frac{\eta}{K_{BP}}\right)\left(1 + S\frac{\gamma}{\eta}T_r\right)(1 + S\tau)} \quad (5)$$

$$\frac{\delta K_v}{\dot{N}}(S) = \frac{K_{\delta K} V\left[S^2 \frac{T_r}{K_{BP}}\left(\gamma + \frac{\sigma d}{v}\right) + S\left(\frac{\eta}{K_{BP}} + \frac{\gamma}{\eta}T_r + \frac{\sigma(b+d)}{V K_{BP}}\right) + 1\right]}{(1 + ST_h)(1 + ST_{pv})\left(1 + S\frac{\eta}{K_{BP}}\right)\left(1 + S\frac{\gamma}{\eta}T_r\right)(1 + S\tau)} \quad (6)$$

Equation (6) gives the transfer function for Fig. 9. The transfer function for Fig. 10 can be similarly calculated or more readily by letting $K_{BP} = 0$ in equation (6). First multiply numerator and denominator of equation (6) by K_{BP}:

$$\frac{\delta K_v}{\dot{N}}(S) = \frac{K_{\delta K} V\left[S^2 T_r\left(\gamma + \frac{\sigma d}{V}\right) + S\left(\eta + \frac{\gamma}{\eta}T_r K_{BP} + \frac{\sigma(b+d)}{V}\right) + K_{BP}\right]}{(1 + ST_h)(1 + ST_{pv})(K_{BP} + S\eta)\left(1 + S\frac{\gamma}{\eta}T_r\right)(1 + S\tau)} \quad (7)$$

Let $K_{BP} = 0$:

$$\frac{\delta K_v}{\dot{N}}(S) = \frac{K_{\delta K} V\left[S^2 T_r\left(\gamma + \frac{\sigma d}{V}\right) + S\left(\eta + \frac{\sigma(b+d)}{V}\right)\right]}{S\eta(1 + ST_h)(1 + ST_{pv})\left(1 + S\frac{\gamma}{\eta}T_r\right)(1 + S\tau)} \quad (8)$$

$$\frac{\delta K_v}{\dot{N}}(S) = \frac{K_{\delta K}\left[V - \frac{\sigma}{\eta}(b+d)\right]\left[1 + S\left(\frac{(V\gamma - \sigma d)T_r}{V\eta - \sigma(b+d)}\right)\right]}{\left(1 + S\frac{\gamma}{\eta}T_r\right)(1 + ST_h)(1 + ST_{pv})(1 + S\tau)} \quad (9)$$

Equation (9) gives the transfer function for Fig. 10.

APPENDIX C

CALCULATION OF THERMODYNAMIC CONSTANTS

$$\eta = \frac{m_1}{p} \quad \frac{m_1}{\theta}\frac{\partial \theta}{\partial p} + \frac{m_1 \frac{\partial h_s}{\partial p}}{h_s - h_w} + \frac{M \frac{\partial h_w}{\partial p}}{h_s - h_w} \quad \text{lb/psi} \tag{1}$$

$$\gamma = \frac{m_1}{p} \quad \frac{m_1}{\theta}\frac{\partial \theta}{\partial p} + \frac{m_1 \frac{\partial h_s}{\partial p}}{h_s - h_w} \quad \text{lb/psi} \tag{2}$$

I. p = 300 psig

$M = 19{,}800$ lb

$m_1 = 369$ lb

$\theta = 422°F = 882°R$

$h_s - h_w = 805$ Btu/lb

$\partial h_w / \partial p = 0.335 \frac{\text{Btu/lb}}{\text{psi}}$

$\partial h_s / \partial p = 0.025 \frac{\text{Btu/lb}}{\text{psi}}$

$\partial \theta / \partial p = 0.31°F/\text{psi}$

$\frac{m_1}{p} = \frac{369}{315} = 1.2$ lb/psi

$-\frac{m_1}{\theta}\frac{\partial \theta}{\partial p} = -\frac{369}{882} \times 0.31 = 0.13$ lb/psi

$\frac{m_1 \frac{\partial h_s}{\partial p}}{h_s - h_w} = \frac{369 \times 0.025}{805} = 0.011$ lb/psi

$\frac{M \frac{\partial h_w}{\partial p}}{h_s - h_w} = \frac{19800 \times 0.335}{805} = 8.24$ lb/psi

$$\eta = 1.2 - 0.13 + 0.011 + 8.24 = 9.32 \text{ lb/psi}$$

$$\gamma = 1.2 - 0.13 + 0.011 = 1.08 \text{ lb/psi}$$

$$\sigma = \frac{1}{h_s - h_w} \text{ lb/Btu}$$

$$= \frac{1}{805} \text{ lb/Btu}$$

$$= 0.00123 \text{ lb/Btu}$$

$$= 0.00123 \times \frac{3.413 \text{ Btu}}{3600 \text{ MW.SEC.}} \times 10^6$$

$$= 1.17 \frac{\text{lb/sec}}{\text{MW}}$$

For 20 MW:

$$\sigma = 1.17 \times 20$$

$$\sigma = 23 \text{ lb/sec @ 20 MW}$$

II. p = 550 psig

By the above methods:

$$\eta = 6.53$$

$$\gamma = 1.05$$

APPENDIX D

EXTRAPOLATION OF FEEDBACK PARAMETERS TO 40 MW

The predicted performance at 40 MW was determined by extrapolating the parameter values using low power data.

"$K_{\delta K}$" and "V" Coefficients

From measurements:

$$(K_{\delta K}\, V)_{20\text{-}550} = 8.9 \text{ db}$$

$$= 2.78$$

$$\frac{(K_{\delta K}\, V)_{20\text{-}550}}{20 \text{ MW}} = \frac{2.78 \times 0.00755 \times 100}{20} \%/\text{MW}$$

$$= 0.106 \%/\text{MW}$$

The value of $(K_{\delta K}\, V)_{40\text{-}550}$ can be obtained by extrapolating Fig. 20 to 40 MW and applying the ratio of slopes at 40 MW and 20 MW to the measured value of $(K_{\delta K}\, V)_{20\text{-}550}$.

0.06% - slope of Fig. 20 at 20 MW

0.042% - slope of Fig. 20 at 40 MW

$$\frac{(K_{\delta K}\, V)_{40\text{-}550}}{40 \text{ MW}} = (0.106\%/\text{MW}) \left(\frac{0.042}{0.06} \right)$$

$$= 0.074 \%/\text{MW}$$

$$(K_{\delta K}\, V)_{40\text{-}550} = \frac{0.074 \times 40}{0.00755 \times 100} = 3.9$$

Since the void condition for 20 MW, 300 psi is similar to that for 40 MW, 550 psi, the predicted $K_{\delta K}\, V$ above was weighted by the value measured in the reduced pressure test:

$$(K_{\delta K}\, V)_{20\text{-}300} = 10.1 \text{ db.}$$

$$= 3.2$$

$$\text{AVERAGE } (K_{\delta K}\, V)_{40\text{-}550} = \frac{(K_{\delta K}\, V)_{40\text{-}550} + (K_{\delta K}\, V)_{20\text{-}330}}{2}$$

$$= 3.6$$

$$(V)_{40-550} = 2.55\ (ft^3/MW)MW \qquad \text{(See Fig. 16)}$$

$$\text{AVERAGE } (K_{\delta K})_{40-550} = \frac{(K_{\delta K}\, V)_{40-550}}{(V)_{40-550}}$$

$$= 1.41$$

$$(V)_{20-300} = 2.19\,(ft^3/MW)MW \qquad \text{(See Fig. 18)}$$

$$(K_{\delta K})_{20-300} = \frac{(K_{\delta K}\, V)_{20-300}}{(V)_{20-300}}$$

$$= 1.46$$

$$(K_{\delta K})_{40-550} = \frac{(K_{\delta K}\, V)_{40-550}}{(V)_{40-550}}$$

$$= 1.53$$

The near equality of the values of $K_{\delta K}$ obtained for 20 MW, 300 psi and 40 MW, 550 psi above verifies the assumption made earlier that reduced pressure tests provide void effects similar to those produced by increasing power at design pressure.

Coefficient "d"

$$d = \frac{M_B \dfrac{\partial h_w}{\partial p}\, \tau}{\rho_s\,(h_s - h_w)} \tag{1}$$

$$(d)_{20-300} = 0.10 \qquad \text{(See IV equation (27))}$$

Assume:

(1) $(\tau)_{40-550} \doteq (\tau)_{20-330}$

(2) $(M_B)_{40-550} \doteq (M_B)_{20-300}$

} By reduced pressure equivalence

$$(d)_{40-550} = \frac{\left(\dfrac{\partial h_w}{\partial p}\right)_{550} (h_s - h_w)_{300}\, (\rho_s)_{300}\, (d)_{20-300}}{\left(\dfrac{\partial h_w}{\partial p}\right)_{300} (h_s - h_w)_{550}\, (\rho_s)_{550}} \tag{2}$$

$$= \frac{0.207 \times 805 \times 0.68 \times 0.010}{0.335 \times 739 \times 1.28}$$

$$= 0.004$$

Coefficient "b"

$$b = \frac{(\dot{M}_{FW} + \dot{M}_R)\frac{\partial h_w}{\partial p}\,\tau\, T_r}{\rho_s\,(h_s - h_w)} \tag{3}$$

$(b)_{20-300} = 0.57$ (See Section IV)

Assume:

(1) $(\dot{M}_{FW} + \dot{M}_R)_{40-550} \doteq (\dot{M}_{FW} + \dot{M}_R)_{20-300}$

(2) $(\tau)_{40-550} \doteq (\tau)_{20-300}$

(3) $(T_r)_{40-550} \doteq (T_r)_{20-300}$

} By reduced pressure equivalence

$$(b)_{40-550} = \frac{\left(\frac{\partial h_w}{\partial p}\right)_{550}(h_s - h_w)_{300}\,(\rho_s)_{300}\,(b)_{20-300}}{\left(\frac{\partial h_w}{\partial p}\right)_{300}(h_s - h_w)_{550}\,(\rho_s)_{550}} \tag{4}$$

$$= \frac{0.207 \times 805 \times 0.68 \times 0.57}{0.335 \times 739 \times 1.28}$$

$$= 0.20$$

Assume:

(1) $(T_h)_{40-550} = (T_h)_{20-300}$

(2) $(T_{pv})_{40-550} = (T_{pv})_{20-300}$

} By reduced pressure equivalence

The above calculations are summarized in Table IV.